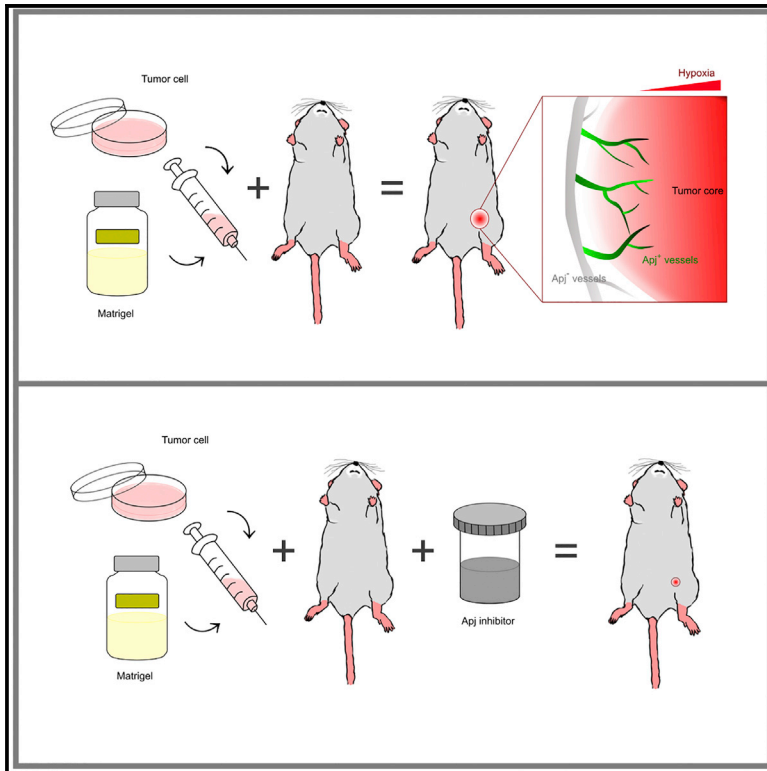


# Cell Reports

## Apj<sup>+</sup> Vessels Drive Tumor Growth and Represent a Tractable Therapeutic Target

### Graphical Abstract



### Authors

Huan Zhao, Xueying Tian, Lingjuan He, ..., Fei Xu, Nicola Smart, Bin Zhou

### Correspondence

zhoubin@sibs.ac.cn

### In Brief

Angiogenesis underpins tumor growth and metastasis, but current targets are suboptimal. Zhao et al. report that Apj is a cell surface marker of pathological angiogenesis and a tractable therapeutic target for tumors.

### Highlights

- Apj is a cell surface marker restricted to pathological angiogenesis
- High expression of Apj in tumor vessels is regulated by hypoxia-VEGF signaling
- Genetic and pharmacological targeting of Apj<sup>+</sup> vessels could inhibit tumor growth



# Apj<sup>+</sup> Vessels Drive Tumor Growth and Represent a Tractable Therapeutic Target

Huan Zhao,<sup>1,2</sup> Xueying Tian,<sup>3</sup> Lingjuan He,<sup>1,2</sup> Yan Li,<sup>1,2</sup> Wenjuan Pu,<sup>1,2</sup> Qiaozhen Liu,<sup>1,2</sup> Juan Tang,<sup>1,2</sup> Jiaying Wu,<sup>1</sup> Xin Cheng,<sup>1</sup> Yang Liu,<sup>4</sup> Qingtong Zhou,<sup>5</sup> Zhen Tan,<sup>6</sup> Fan Bai,<sup>4</sup> Fei Xu,<sup>5,7</sup> Nicola Smart,<sup>8</sup> and Bin Zhou<sup>1,2,3,7,9,\*</sup>

<sup>1</sup>The State Key Laboratory of Cell Biology, CAS Center for Excellence in Molecular Cell Science, Shanghai Institute of Biochemistry and Cell Biology, Chinese Academy of Sciences, University of Chinese Academy of Sciences, Shanghai, 200031, China

<sup>2</sup>Key Laboratory of Nutrition and Metabolism, Institute for Nutritional Sciences, Shanghai Institutes for Biological Sciences, University of Chinese Academy of Sciences, Chinese Academy of Sciences, Shanghai, 200031, China

<sup>3</sup>Key Laboratory of Regenerative Medicine of Ministry of Education, Jinan University, Guangzhou, 510632, China

<sup>4</sup>Biodynamic Optical Imaging Center (BIOPI), School of Life Sciences, Peking University, Beijing, 100871, China

<sup>5</sup>Human Institute, ShanghaiTech University, Shanghai, 201210, China

<sup>6</sup>Department of Pediatric Hematology/Oncology, Xinhua Hospital Affiliated to Shanghai Jiao Tong University, School of Medicine, Shanghai, 200092, China

<sup>7</sup>School of Life Science and Technology, ShanghaiTech University, Shanghai, 201210, China

<sup>8</sup>British Heart Foundation Centre of Regenerative Medicine, Department of Physiology, Anatomy and Genetics, University of Oxford, Oxford, UK

<sup>9</sup>Lead Contact

\*Correspondence: [zhoubin@sibs.ac.cn](mailto:zhoubin@sibs.ac.cn)

<https://doi.org/10.1016/j.celrep.2018.10.015>

## SUMMARY

Identification of cellular surface markers that distinguish tumorous from normal vasculature is important for the development of tumor vessel-targeted therapy. Here, we show that Apj, a G protein-coupled receptor, is highly enriched in tumor endothelial cells but absent from most endothelial cells of adult tissues in homeostasis. By genetic targeting using *Apj-CreER* and *Apj-DTRGFP-Luciferase*, we demonstrated that hypoxia-VEGF signaling drives expansion of Apj<sup>+</sup> tumor vessels and that targeting of these vessels, genetically and pharmacologically, remarkably inhibits tumor angiogenesis and restricts tumor growth. These *in vivo* findings implicate Apj<sup>+</sup> vessels as a key driver of pathological angiogenesis and identify Apj<sup>+</sup> endothelial cells as an important therapeutic target for the anti-angiogenic treatment of tumors.

## INTRODUCTION

Angiogenesis underpins tumor growth and metastasis (Ferrara and Kerbel, 2005; Augustin and Koh, 2017). Inhibiting or destroying tumor angiogenesis has emerged as a major therapeutic strategy for the treatment of tumors in various preclinical and clinical studies (Heath and Bicknell, 2009). Current targets for inhibiting angiogenesis, such as vascular endothelial growth factor (VEGF), play fundamental roles in both pathological and physiological conditions, therefore exposing healthy vessels to adverse off-target effects of anti-angiogenic treatment (Lohela et al., 2009). Thus, the identification of alternative cell surface markers that positively discriminate pathological angiogenesis, such as in

tumor blood vessels, from stable vessels is urgently needed to selectively target pathological angiogenesis.

Serial analysis of gene expression on isolated endothelial cells identified Apelin to be overexpressed in tumor vessels versus normal endothelium (Seaman et al., 2007). The Apelin receptor, Apj, is a G protein-coupled trans-membrane receptor expressed on the endothelial cell surface (Cox et al., 2006). Apelin is a potent angiogenic factor that is required for normal embryonic vascular development (Schulze et al., 2015; Cox et al., 2006) and functions downstream of VEGFA (Kálin et al., 2007; Charo et al., 2009). Apelin deficiency attenuated hypoxia-induced retinal angiogenesis, despite the upregulation of VEGF, and Apelin inhibition suppressed endothelial cell proliferation without affecting the VEGF/VEGF receptor 2 signaling pathway (Kasai et al., 2004). The Apelin/Apj system is also reported to promote maturation of tumor vasculature and improve the efficiency of immune therapy (Kidoya et al., 2012) and to regulate blood vessel caliber (Kidoya et al., 2008). In addition to these regulatory functions in the vasculature, the Apelin-Apj axis also mediates heart contractility and blood pressure regulation (Dai et al., 2006; Ashley et al., 2005). Mechanistically, Apelin, via Apj, increases angiotensin-converting enzyme 2 in failing hearts and functions as an inotropic and cardioprotective peptide to improve heart functions (Sato et al., 2013). Although Apelin is highly enriched in endothelial cells during development, it is significantly reduced in endothelial cells of adult organs (Liu et al., 2015). Only under pathological conditions, such as myocardial infarction or tumor growth, is Apelin increased in endothelial cells (Sheikh et al., 2008; Liu et al., 2015). Given its diverse actions on cardiovascular health and disease, the Apelin-Apj axis has emerged as a promising therapeutic candidate (Barnes et al., 2010).

Previous work has demonstrated that Apelin-expressing tumor endothelial cells can be efficiently targeted, using a genetic approach, to restrict tumor growth (Liu et al., 2015). However, as



a secreted peptide, Apelin presents a challenge for pharmacological therapies, whereas its receptor, Apj, is expressed on the cell surface and may be more tractable for selectively targeting tumors with small-molecule antagonists. Apj has diverse roles in cardiovascular diseases as aforementioned. During development, Apj is also the receptor for Elabela (Ela), which plays a critical role in heart development (Chng et al., 2013), and Toddler, which promotes cell movement during gastrulation (Pauli et al., 2014). Mechanistically, Apj acts as a specific rheostat for the Nodal/TGF $\beta$  pathway during early stages of cardiogenesis to ensure heart formation (Deshwar et al., 2016) and acts downstream of the Cripto signaling pathway to govern mesoderm patterning and cardiac specification in mammals (D'Aniello et al., 2009). In addition to its role in modulating endothelial MEF2 activation (Kang et al., 2013), Apj in venous endothelial cells regulates parallel arterial-venous alignment in the skin (Kidoya et al., 2015) and promotes the maturation and growth of astrocytes in the retina (Sakimoto et al., 2012). Postnatally, Apj acts as a mechanosensor, with activation leading to cardiac hypertrophy (Scimia et al., 2012); yet conversely, Apj exerts a hypotensive effect *in vivo* by countering the pressure elevation induced by angiotensin II (Ishida et al., 2004).

In addition to its cardiovascular functions, Apj activation in some cancers suggests a possible function in tumor formation. Previous cancer profiling array analyses showed that Apj is upregulated in human colon adenomas and adenocarcinomas (Picault et al., 2014). A recent study on somatic gene mutations in cancer cells identified multiple loss-of-function mutations in Apj in patient tumors that were refractory to immunotherapy (Patel et al., 2017). Beyond its potential to mark tumor cells for therapeutic targeting, the high expression of Apj in tumor blood vessels warrants further investigation. Because the tumor microenvironment is highly hypoxic, and hypoxia induces Apelin/Apj-driven endothelial cell proliferation and regenerative angiogenesis (Eyries et al., 2008), we reasoned that Apj<sup>+</sup> vessels could likewise be responsive to tumor hypoxia and critical for tumor growth. In this study, we find that Apj expression is induced in hypoxic tumor endothelial cells, in experimental tumor models as well as in human tumors. We demonstrate that expansion of Apj<sup>+</sup> vessels during tumor development is regulated by hypoxia-VEGF signaling. Finally, our work demonstrates, by genetic cell ablation and using a small peptide Apj antagonist peptide, that Apj<sup>+</sup> vessels can be targeted to inhibit tumor progression, without affecting vessel integrity in other organs. Thus, we identify Apj as a cell surface marker of pathological angiogenesis, such as that which drives tumor growth, which may be exploited as a therapeutic target for the anti-angiogenic treatment of tumors.

## RESULTS

### Apj Is Expressed in Blood Vessels at Embryonic Stages but Is Reduced in Adult Tissues

To delineate the map of Apj receptor expression in development and disease, we generated an *Apj-CreER* knockin mouse to mark Apj<sup>+</sup> cells. Through homologous recombination using CRISPR/Cas9, we generated an *Apj-CreER* knockin allele by replacing the translational start codon ATG of the endogenous *Apj*

gene (Figure 1A). We then crossed *Apj-CreER* with a responsive reporter line, *R26-GFP*, to generate the *Apj-CreER;R26-GFP* mouse, which we treated with tamoxifen to induce Cre-loxP recombination and labeling of Apj<sup>+</sup> cells (Figure 1B). By tamoxifen induction at embryonic day (E) 14.5 and tissue collection at E16.5 for analysis, we found that GFP (a surrogate for Apj<sup>+</sup> cells) was restricted to vascular endothelial cells in multiple embryonic tissues, including heart, brain, lung, liver, intestine, and kidney (Figure S1). To examine *Apj* expression in adult tissues, we treated 8- to 10-week old *Apj-CreER;R26-GFP* mice with tamoxifen and collected tissue samples 10 days later for analysis (Figure 1C). Immunostaining for GFP and endothelial cell marker PECAM on tissue sections showed sparse Apj<sup>+</sup> cells compared with their embryonic counterparts (Figures 1D and S1). We detected only rare GFP signals in tissues from mice without tamoxifen treatment, indicating negligible leakiness of *Apj-CreER*. The above data confirm that *Apj* is specifically expressed in vascular endothelial cells in the developing embryo, and its expression is significantly reduced by adulthood.

### Apj Is Highly Enriched in Adult Tumor Blood Vessels

As Apelin is induced in pathological conditions such as tissue ischemia (Liu et al., 2015), we reasoned that Apj, as its receptor, might also be upregulated under hypoxic conditions, such as tumor formation. To directly visualize the Apj<sup>+</sup> cells, we took advantage of *Apj-CreER* to label Apj<sup>+</sup> cells during tumor growth. We set up a series of xenograft tumor models using tumor cell lines TC-1, Hepa1-6, and LLC mixed with Matrigel and treated *Apj-CreER;R26-GFP* mice with tamoxifen after tumor implantation. Tumors, as well as other tissue samples, were collected at 10 days after implantation (Figure 2A). We detected few vascular endothelial cells labeled by *Apj-CreER* in healthy tissues, including heart, brain, lung, and liver (Figure 2B), consistent with the data above showing scarce Apj<sup>+</sup> cells in adult tissues. In contrast, the majority of vascular endothelial cells were GFP<sup>+</sup> in tumor samples, with the percentage of GFP<sup>+</sup> endothelial cells being  $97.66 \pm 0.59\%$ ,  $95.28 \pm 0.67\%$ , and  $96.08 \pm 0.88\%$  in TC-1, Hepa1-6, and LLC implanted tumors, respectively (Figures 2B–2E). H&E staining on TC-1 tumor section from *Apj-CreER;R26-GFP* mice showed clear boundaries and homogeneous density of tumor tissues (Figure S2A). By immunostaining for GFP and PECAM, we found that most of the ECs in tumors were GFP<sup>+</sup>, while few of the endothelial cells (ECs) in paratumorous tissues were GFP<sup>+</sup> (Figures S2B and S2C). To better characterize these labeled vessels in tumors, we performed immunostaining for genetic marker GFP, EC marker PECAM, and different smooth muscle markers on sections of tumors. We found that only a minority of GFP<sup>+</sup> ECs were surrounded by smooth muscle cells (Figure S2D), consistent with the viewpoint that most tumor vessels are immature and unstable. We also injected BS1-lectin to tamoxifen-injected *Apj-CreER;R26-GFP* mice and found that most GFP<sup>+</sup> vessels were also BS1-lectin<sup>+</sup>, indicating that they are capable of perfusion (Figure S2E). We also generated an orthotopic tumor model by injecting hepatic cancer cells (Hepa1-6) directly into the livers of *Apj-CreER;R26-GFP* mice. Immunostaining for GFP and PECAM showed a significantly higher percentage of GFP<sup>+</sup> vessels in orthotopic tumors than surrounding healthy liver tissues (Figures



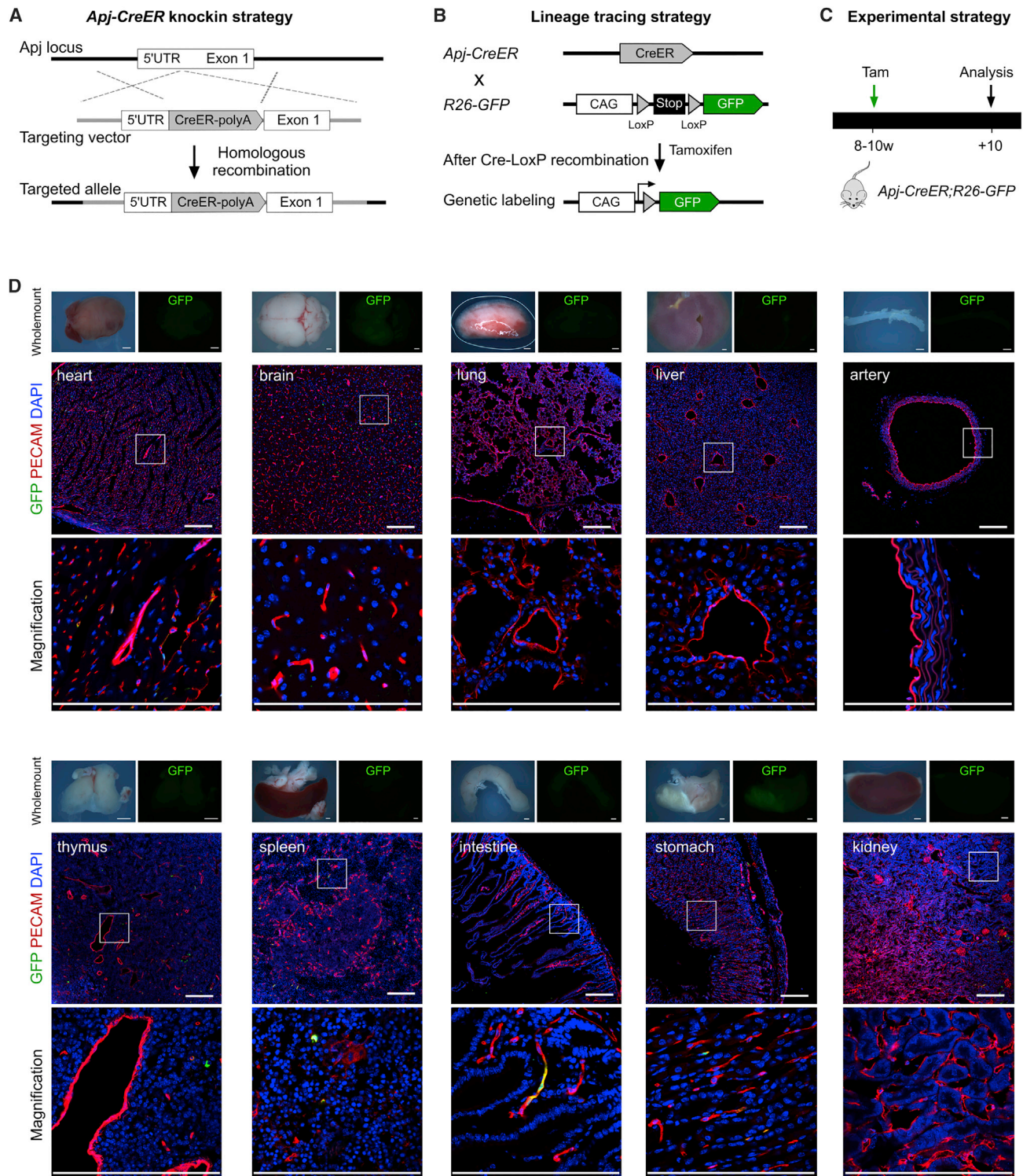


**Figure 1. *Apj-CreER* Sparsely Labeled Endothelial Cells in Adult Organs**

(A) Strategy for generation of *Apj-CreER* knockin allele.

(B) Schematic figure showing genetic lineage tracing strategy.

(C) Experimental strategy for tamoxifen induction and tissue collection.

(D) Immunostaining for GFP and PECAM on tissue sections. The whole-mount images of bright-field and fluorescence of each organ are shown above. Boxed regions are magnified at the bottom. Scale bars, 1 mm in whole-mount images and 200  $\mu$ m in sections. Each image is representative of five individual samples.



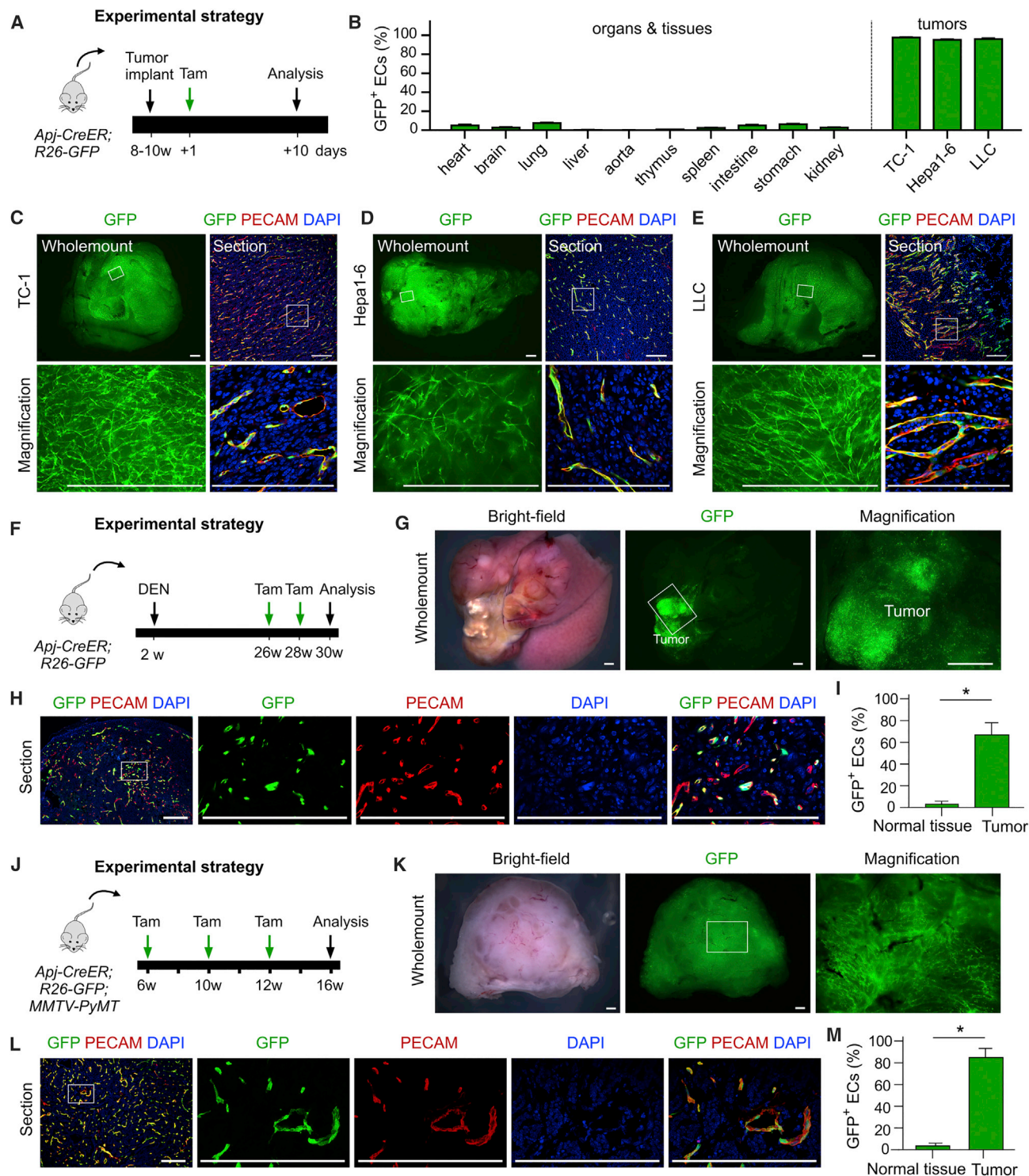


**Figure 2. *Apj-CreER* Labeled the Majority of Endothelial Cells in Xenograft Tumors, Chemically Induced Tumors, and Spontaneous Tumors**

(A) Experimental strategy for tamoxifen induction and tissue collection.

(B) Quantification of the percentage of GFP<sup>+</sup> endothelial cells in different organs and three xenograft tumor models. Data are mean  $\pm$  SEM; n = 5.

(C–E) Whole-mount fluorescence images of xenograft tumors (left). Immunostaining for GFP and PECAM on tumor sections (right). Boxed regions are magnified in the lower panel. (C) TC-1, (D) Hepa1-6, and (E) LLC.

(F) Experimental strategy for DEN-induced liver tumor model and time schedule for tamoxifen induction and tissue analysis.

(G) Whole-mount bright-field and fluorescence images of chemical induced tumor tissues. Boxed region is magnified on the right.

(legend continued on next page)

S2F–S2H). These data demonstrate that *Apj* receptor is highly enriched in vascular ECs of implanted tumors.

To strengthen the above finding, and to analyze *Apj*<sup>+</sup> cells in more physiologically relevant tumor angiogenesis models, we used spontaneous tumor formation models by chemically induced liver cancer and genetically modified mammary cancer models. Diethylnitrosamine (DEN)-treated mice have grossly visible tumors at 30 weeks, so we treated mice with tamoxifen to label *Apj*<sup>+</sup> vessels at 4 and 2 weeks prior to sample collection (Figure 2F). Whole-mount epifluorescence revealed an enrichment of the GFP signal in the tumor compared with other regions of *Apj-CreER;R26-GFP* liver (Figure 2G). In sections, we confirmed a significantly higher percentage of GFP<sup>+</sup> ECs in tumor compared with surrounding liver tissues ( $67.82 \pm 9.55\%$  versus  $2.01 \pm 1.84\%$  in tumor and normal tissue, respectively; Figures 2H and 2I). For the mammary tumor study, we crossed *Apj-CreER;R26-GFP* with *MMTV-PyMT* (Guy et al., 1992), a murine breast cancer model driving polyomavirus middle T-antigen in the mammary gland, in order to trace *Apj*<sup>+</sup> cells in tumors (Figure 2J). Whole-mount epifluorescence (Figure 2K) and sectional staining (Figure 2L) of mammary tumors consistently showed GFP<sup>+</sup> cells to be highly enriched in ECs and significantly more abundant in tumor vessels compared with those in healthy mammary gland ( $81.85 \pm 9.21\%$  versus  $1.98 \pm 1.45\%$  in tumor and normal tissue, respectively; Figure 2M).

### Hypoxia-VEGF Signaling Regulates *Apj*<sup>+</sup> Vessel Expansion in Tumors

To understand the mechanism that drives increased *Apj* expression in tumor vessels, but not in healthy tissues, we analyzed tissue hypoxia and also cell proliferation of implanted tumors (Figure 3A). Immunostaining for Hypoxyprobe and GFP on tumor samples showed two distinct regions: tumor periphery that was less hypoxic and rich with GFP<sup>+</sup> vessels and tumor core that was highly hypoxic and poorly vascularized (Figure 3B). Because GFP acts as a genetic lineage tracing marker, any ECs that had a history of *Apj* expression would be GFP<sup>+</sup>. The descendants of *Apj*<sup>+</sup> cells may have subsequently lost *Apj* expression but retain the genetic tracer GFP. Immunostaining of GFP and ESR, as a surrogate for *Apj*-expressing cells that remain positive for CreER, on tumor tissue sections showed that ESR/*Apj* was enriched in ECs that were located in the region close to the tumor core rather than the peripheral region (Figure 3C), suggesting that hypoxia may affect *Apj* expression in ECs. To directly prove this, we cultured human umbilical vein ECs (HUVECs) under low oxygen and found that *Apj* protein was significantly increased in hypoxic compared with normal condition ( $18.57 \pm 1.98$  versus  $1.00 \pm 0.83$ , respectively; Figures 3D and 3E). Immunostaining for EdU, GFP, and PECAM showed that a substantial number of

GFP<sup>+</sup> ECs incorporated EdU, indicating a high proliferation of *Apj*<sup>+</sup> vessels and their angiogenic expansion for tumor growth (Figure 3F). These data demonstrate that *Apj*<sup>+</sup> vessels are recruited to hypoxic regions during tumor growth, with *Apj* expression in vascular ECs regulated by tumor hypoxia.

To further explore whether hypoxia regulates *Apj* expression, we used two ischemia models: hindlimb ischemia and myocardial infarction (MI), to examine *Apj* expression. We performed femoral artery ligations in *Apj-CreER;R26-GFP* adult mice to establish a model of hindlimb ischemia injury and induce a hypoxic environment in hindlimb tissue. We administered tamoxifen 1 day after surgery and collected tissues adjacent to the femoral artery 15 days later (Figure S3A). Whole-mount fluorescence and immunostaining data showed that the vast majority of newly generated ECs were labeled by the genetic marker GFP, compared with ECs in sham-operated hindlimb ( $83.67 \pm 9.81\%$  versus  $2.03 \pm 1.84\%$ , respectively; Figures S3B–S3E). We also performed MI on *Apj-CreER;R26-GFP* and injected tamoxifen 1 day after surgery. We analyzed heart tissues 15 days later and found that a substantial number of ECs in the injured tissue were GFP<sup>+</sup>, compared with sham controls ( $61.22 \pm 11.38\%$  versus  $7.25 \pm 5.06\%$ , respectively; Figures S3F–S3I). These data demonstrate that *Apj* expression is increased in ECs when tissue becomes ischemic and/or hypoxic.

We next sought to address the molecular mechanism that controls expansion of *Apj*<sup>+</sup> vessels in tumors. As hypoxia induces VEGFA expression through hypoxia-inducible factor (HIF) 1α (Liu et al., 1995; Forsythe et al., 1996; Ryan et al., 1998), we speculated that VEGFA signaling controls *Apj*<sup>+</sup> vessel expansion in tumors. We therefore generated *Apj-CreER;R26-GFP;Kdrfl/fl* mice for loss of VEGFR2 expression in *Apj*<sup>+</sup> vessels and used *Apj-CreER;R26-GFP;Kdrfl/+* littermate controls for direct comparison. We treated mice with tamoxifen at 3 days following tumor implantation and collected tissues for analysis after 10 days (Figure 4A). Tamoxifen induction resulted in Cre-loxP-mediated *Kdr* gene deletion, leading to loss of VEGFR2 expression in *Apj*<sup>+</sup> ECs (Figure 4B). The tumor volume increased significantly in *Apj-CreER;R26-GFP;Kdrfl/+* mice, but the tumors on *Apj-CreER;R26-GFP;Kdrfl/fl* mice did not increase, and there was a significant difference in tumor volume between the two groups from day 5 onward (Figure 4C). We collected tumor samples at day 10 and found that both tumor volume ( $49.50 \pm 12.70$  versus  $200.2 \pm 30.91$  versus  $205.35 \pm 38.11$  mm<sup>3</sup>) and weight ( $163.22 \pm 15.51$  versus  $518.30 \pm 79.72$  versus  $574.95 \pm 118.31$  mg) were significantly reduced in *Apj-CreER;R26-GFP;Kdrfl/fl* mice (tamoxifen treated) compared with *Apj-CreER;R26-GFP;Kdrfl/+* mice (tamoxifen treated) or *Apj-CreER;R26-GFP;Kdrfl/fl* without tamoxifen treatment (Figures 4D–4F). By lineage tracing of *Apj*<sup>+</sup> vessels, we found a significant reduction in GFP<sup>+</sup> signals

(H) Immunostaining for GFP and PECAM on sections of tumor tissues in (G). Boxed region is magnified on the right.

(I) Quantification of the percentage of GFP<sup>+</sup> endothelial cells in normal liver tissues and chemically induced tumors. \**p* < 0.05. Data are mean ± SEM; *n* = 5.

(J) Experimental strategy for spontaneous mammary gland tumor model using *Apj-CreER;R26-GFP;MMTV-PyMT* mice and time schedule for tamoxifen induction and tissue analysis.

(K) Whole-mount bright-field and fluorescence view of spontaneous tumor tissues. Boxed region is magnified on the right.

(L) Immunostaining for GFP and PECAM on sections of tumor tissues in (K). Boxed region is magnified on the right.

(M) Quantification of the percentage of GFP<sup>+</sup> endothelial cells in normal mammary gland tissues and tumors. \**p* < 0.05. Data are mean ± SEM; *n* = 5.

Scale bars, 1 mm in whole-mount images and 200 μm in sections. Each image is representative of five individual samples.



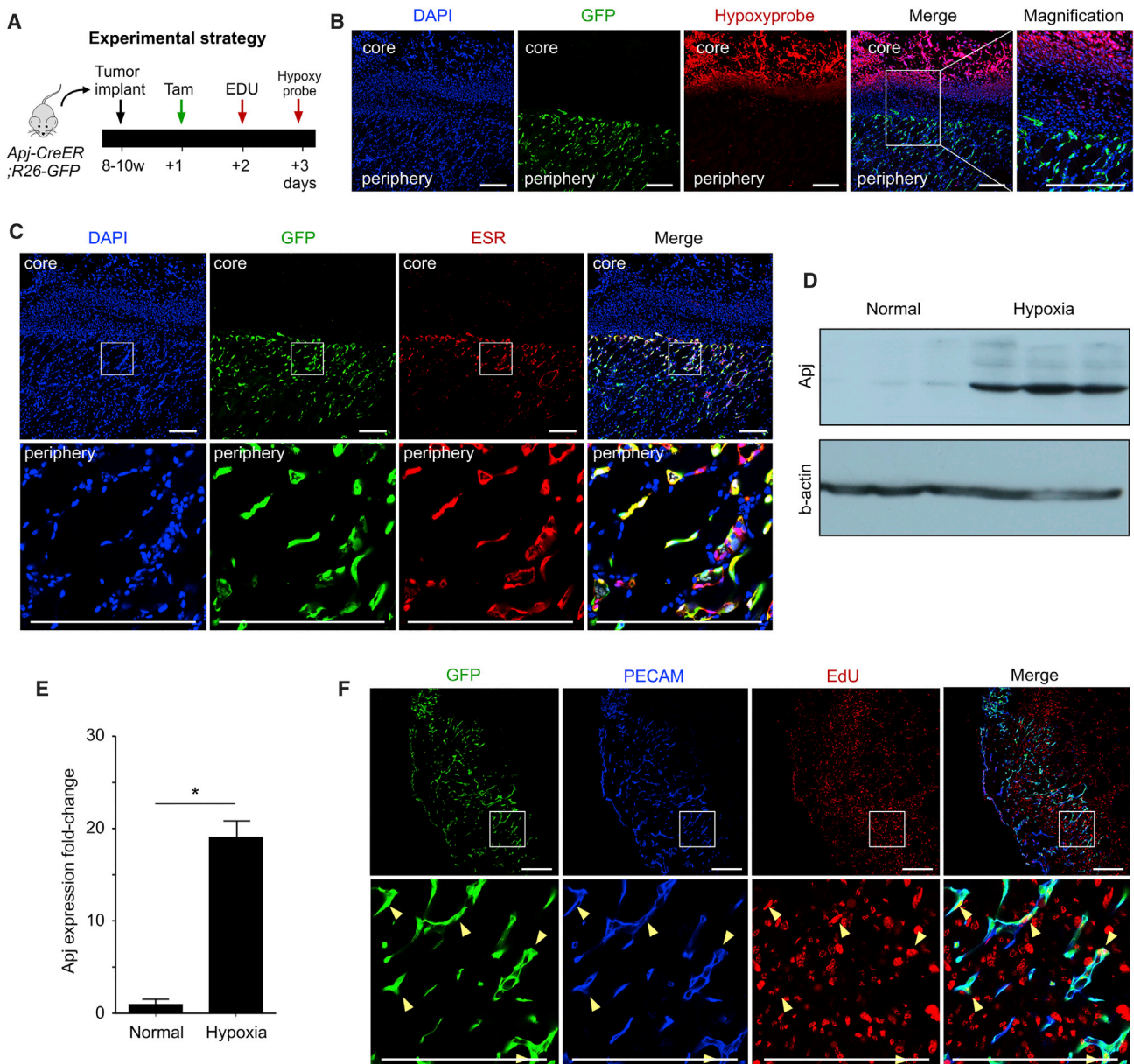


**Figure 3. Apj Expression Is Controlled by Hypoxia and Is Enriched in Hypoxic Tumor**

(A) Schematic figure showing experimental strategy for induction of EDU and Hypoxyprobe.

(B) Immunostaining for GFP and Hypoxyprobe on tumor section.

(C) Immunostaining for GFP and ESR on tumor section shows that Apj expression is highly enriched in the region adjacent to tumor core.

(D and E) Western blot of Apj protein from HUVECs cultured under normal or hypoxia conditions (D) and quantification of Apj expression (E). \* $p < 0.05$ . Data are mean  $\pm$  SEM;  $n = 3$ .

(F) Immunostaining for GFP, PECAM, and EdU on tumor section. Arrowheads indicate proliferating endothelial cells marked by Apj.

Scale bars, 200  $\mu$ m.

in tumors from *Apj-CreER;R26-GFP;Kdrfl/fl* mice but not in tumors from *Apj-CreER;R26-GFP;Kdrfl/+* mice (Figure 4G). Immunostaining for PECAM showed a significant reduction in PECAM<sup>+</sup> vascular EC density in tumors of *Apj-CreER;R26-GFP;Kdrfl/fl* mice, compared with those of *Apj-CreER;R26-GFP;Kdrfl/+* mice ( $9.83 \pm 1.96$  versus  $30.50 \pm 6.72$  per 63 $\times$  field

in tumors from mutant and control, respectively (Figures 4H and 4I). We did not detect any observable decrease in vessel density or morphological changes (Figure S4) in other organs or tissues examined. Collectively, these data demonstrate that hypoxia regulates *Apj* expression and that hypoxia-VEGF signaling controls expansion of Apj<sup>+</sup> vessels in tumor formation.



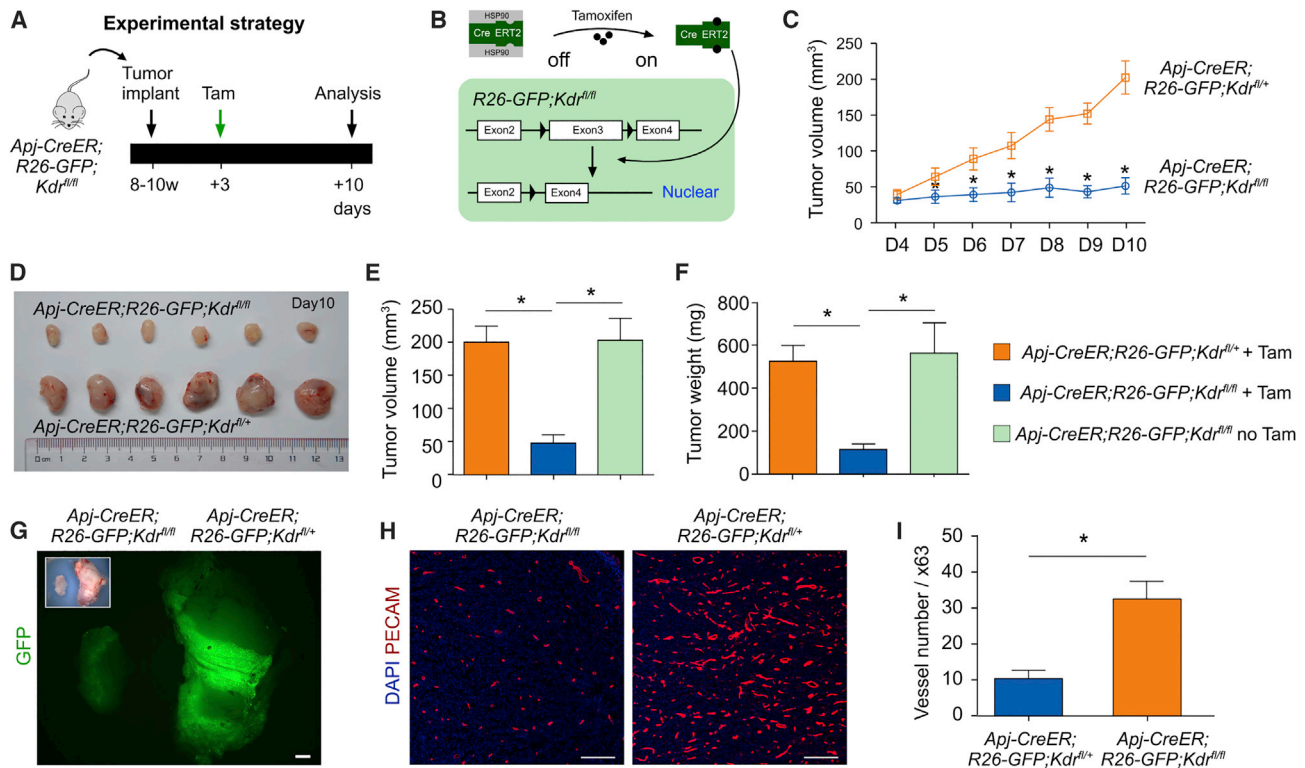


**Figure 4. Expansion of *Apj*<sup>+</sup> Vessels in Tumor Growth Is Regulated by VEGF Signaling**

(A and B) Schematic figure showing experimental strategy (A) and working principle for CreER-induced ablation of VEGFR2 (*Kdr*) gene (B). (C) Quantification of tumor volume (length  $\times$  width<sup>2</sup>/2 [mm<sup>3</sup>]) at various times after implantation. \**p* < 0.05. Data are mean  $\pm$  SEM; *n* = 6. (D) Image of tumors collected from *Apj-CreER;R26-GFP;Kdr<sup>fl/fl</sup>* mice or *Apj-CreER;R26-GFP;Kdr<sup>fl/+</sup>* mice treated with tamoxifen. (E and F) Quantification of tumor volume (E) and tumor weight (F) of three different groups as indicated. \**p* < 0.05. Data are mean  $\pm$  SEM; *n* = 6. (G) Whole-mount fluorescence view of GFP<sup>+</sup> tumors. Inset is bright-field image. (H) Immunostaining for PECAM on tissue sections. (I) Quantification of vessel number per field (63 $\times$ ). \**p* < 0.05. Data are mean  $\pm$  SEM; *n* = 6. Scale bars, 1 mm in whole-mount and 200  $\mu$ m in others. Each image is representative of six individual samples.

### In Vivo Monitoring and Genetic Ablation of *Apj*<sup>+</sup> Vessels

To permit *in vivo* monitoring of the *Apj*<sup>+</sup> vessels in tumors, we generated an *Apj* knockin mouse allele by targeting DTRGFP and luciferase into the endogenous ATG of the *Apj* gene, by homologous recombination using CRISPR/Cas9 (Figure 5A). Most vascular ECs across multiple organs, including kidney, pancreas, heart, and brain, remain GFP negative, confirming minimal activity of *Apj* in blood vessels of adult organs (Figure 5B). In contrast, GFP and diphtheria toxin receptor (DTR) were readily detected in most PECAM<sup>+</sup> ECs in the tumor (Figure 5C), indicating activation of *Apj* in tumor blood vessels. To non-invasively monitor the *Apj*<sup>+</sup> cells *in vivo*, rather than by obtaining tissues *post mortem*, we used a bioluminescent imaging system and detected luciferase activity in the tumors of *Apj-DTRGFP-Luc* mice (Figure 5D). We did not detect any noticeable signals in implanted tumors of wild-type mice, indicating that the luminescent signals in the tumor derived from *Apj*<sup>+</sup> host ECs.

To functionally test if these *Apj*<sup>+</sup> vessels were required to drive tumor growth, we used two independent strategies to ablate *Apj*<sup>+</sup> vessels. Because tumor vessels were active for *Apj* and DTRGFP, we injected diphtheria toxin (DT) to assess whether

DT mediated EC death would affect tumor growth (Figure 5E). After DT binds to DTR, the A subunit of DT (DTA) inactivates elongation factor 2 (EEF2), preventing protein synthesis and rapidly leading to cell death (Palmiter et al., 1987; Breitman et al., 1987). Tumor growth in DT-injected *Apj-DTRGFP-Luc* mice was significantly impaired compared with PBS-injected mice (Figures 5F and 5G). Additionally, tumor weight was significantly reduced after DT treatment compared with PBS (164.6  $\pm$  20.17 versus 352.0  $\pm$  24.78 mg in DT and PBS groups, respectively; Figure 5H). Immunostaining for GFP, DTR, and PECAM confirmed that there were significantly fewer vessels in DT-treated tumor compared with the PBS group (14.06  $\pm$  6.22 versus 49.82  $\pm$  4.85 for density in DT and PBS groups, respectively; Figures 5I and 5J). The inhibition of vessel growth was specific to the tumor, as we did not detect any noticeable dropout of vessel density or impaired tissue morphogenesis in other organs in the DT-treated group in comparison with the PBS-treated group (Figure S5).

For the second strategy, we used *Apj-CreER* to induce DTA in *Apj*-derived lineages by tamoxifen (Tam) administration. We generated *Apj-CreER;R26-GFP/DTA* triple-positive mice and

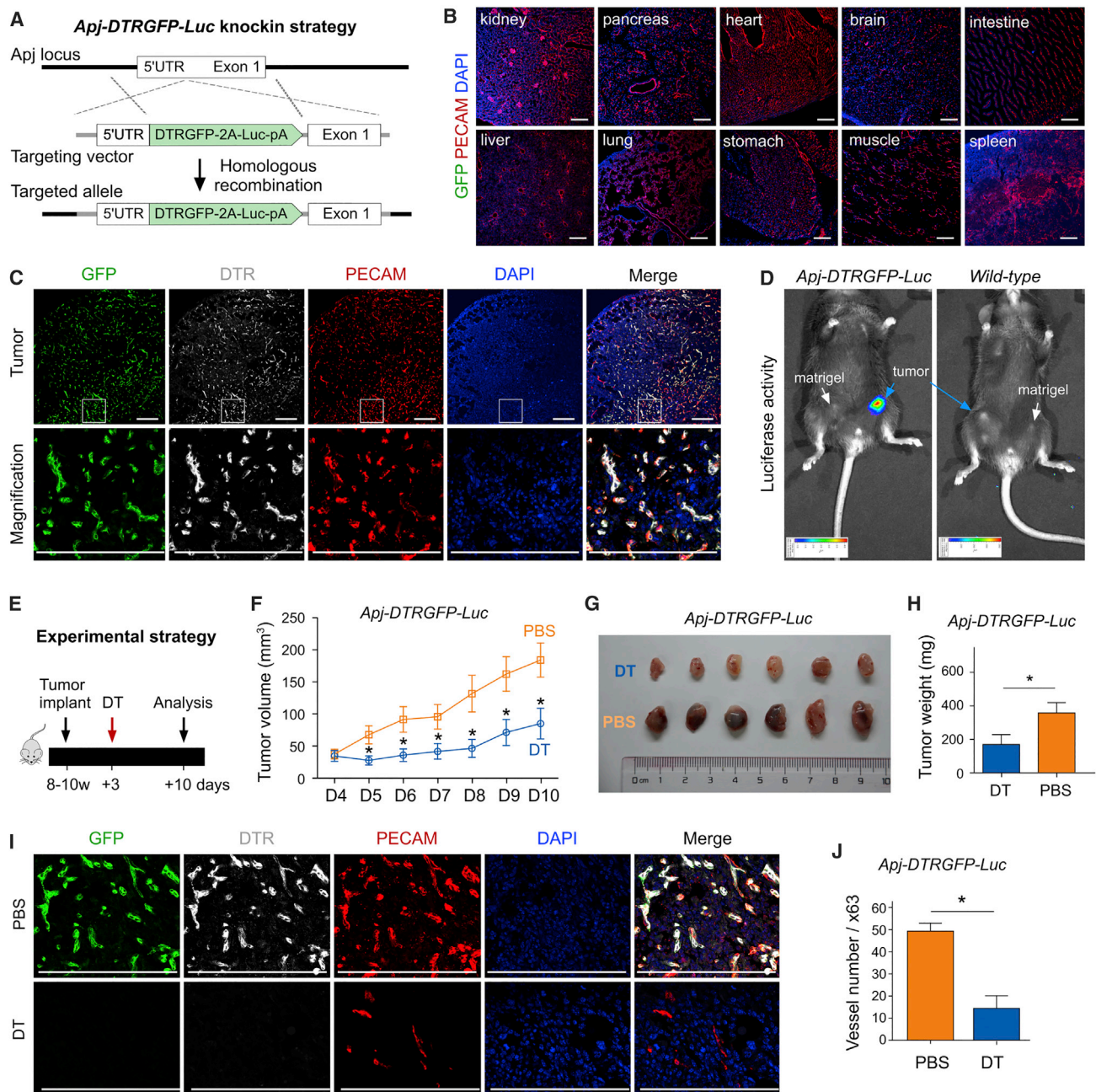


**Figure 5. Generation and Characterization of *Apj-DTRGFP-Luc* Mouse Line**

(A) Schematic figure showing strategy for generation of *Apj-DTRGFP-Luc* allele by homologous recombination using CRISPR/Cas9.

(B) Immunostaining for GFP and PECAM on tissue sections of *Apj-DTRGFP-Luc* mouse organs.

(C) Immunostaining for GFP, DTR, and PECAM on tumor section of the same mouse.

(D) One minute luminescent images of *Apj-DTRGFP-Luc* and littermate wild-type mouse after tumor (blue arrows) or Matrigel (white arrows) implantation.

(E) Schematic figure showing experimental strategy. DT, diphtheria toxin.

(F) Quantification of tumor volume (length  $\times$  width<sup>2</sup>/2 [mm<sup>3</sup>]) at various times after tumor implantation. \* $p < 0.05$ . Data are mean  $\pm$  SEM;  $n = 6$ .

(G) Picture of tumors from *Apj-DTRGFP-Luc* mice treated with DT or PBS.

(H) Quantification of tumor weight of two different groups as indicated. \* $p < 0.05$ . Data are mean  $\pm$  SEM;  $n = 6$ .

(I) Immunostaining for GFP, DTR, and PECAM on tumors collected from *Apj-DTRGFP-Luc* mouse treated with DT or PBS.

(J) Quantification of vessel number per 63 $\times$  field. \* $p < 0.05$ . Data are mean  $\pm$  SEM;  $n = 6$ . Scale bars, 200  $\mu$ m.

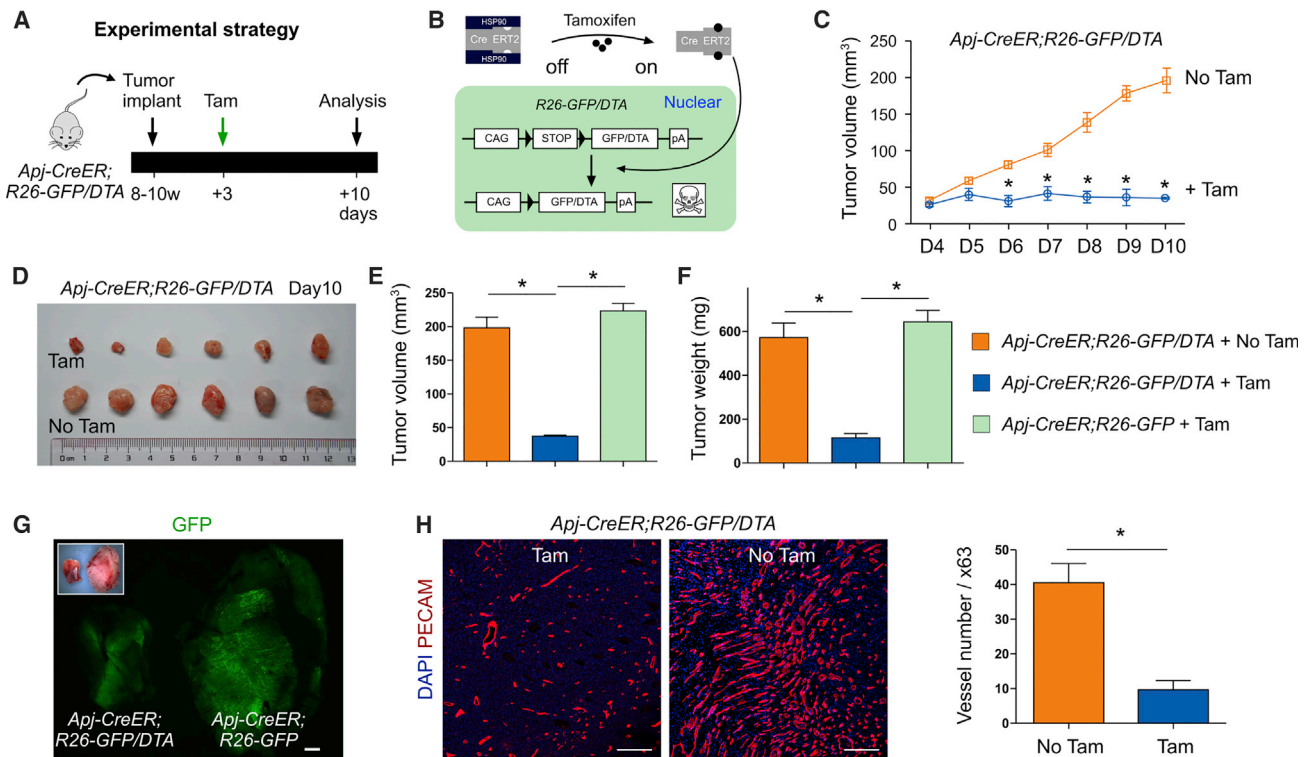


**Figure 6. Genetic Ablation of *Apj*<sup>+</sup> Vessels Significantly Reduced Tumor Growth**

(A and B) Schematic figure showing experimental strategy (A) and working principle for CreER-induced DTA expression for cell death (B). (C) Quantification of tumor volume (length  $\times$  width<sup>2</sup>/2 [mm<sup>3</sup>]) at various times after implantation. \* $p < 0.05$ . Data are mean  $\pm$  SEM;  $n = 6$ . (D) Picture of tumors from *Apj-CreER;R26-GFP/DTA* mice treated with tamoxifen (+ Tam) or corn oil (no Tam). (E and F) Quantification of tumor volume (E) and tumor weight (F) of three different groups as indicated. \* $p < 0.05$ . Data are mean  $\pm$  SEM;  $n = 6$ . (G) Whole-mount fluorescence view of GFP<sup>+</sup> tumors. Inset is bright-field view. (H) Immunostaining for PECAM on tissue sections and quantification of their number per 63 $\times$  field. \* $p < 0.05$ . Data are mean  $\pm$  SEM;  $n = 6$ . Scale bars, 1 mm in whole-mount and 200  $\mu$ m in others. Each image is representative of six individual mouse samples.

injected Tam to induce Cre-loxP-mediated DTA expression in *Apj*<sup>+</sup> cells (Figures 6A and 6B). As an internal control, we treated *Apj-CreER;R26-GFP/DTA* littermate mice with corn oil (no Tam). After Tam treatment, tumor volume did not increase over the 10 days post-transplantation, compared with elevated tumor volume in the no Tam group (Figure 6C). Tumor samples collected at day 10 after implantation showed a significant increase in tumor size ( $198.47 \pm 18.16$  versus  $215.52 \pm 14.59$  versus  $45.22 \pm 3.21$  mm<sup>3</sup>), as well as tumor weight ( $587.29 \pm 61.12$  versus  $618.09 \pm 46.20$  versus  $115.50 \pm 11.15$  mg), in the no Tam group and Tam-treated no DTA group, compared with the Tam group (Figures 6D–6F). We also observed fewer GFP<sup>+</sup> cells in tumors of DTA mice, compared with controls, after Tam treatment (Figure 6G). The blood vessel density in the Tam group was significantly reduced compared with the no Tam group ( $40.06 \pm 7.92$  versus  $9.20 \pm 2.35$  for density in the no Tam and Tam groups, respectively; Figure 6H). This growth inhibition phenotype was restricted to the tumor, as we did not detect any noticeable dropout of vessel density or morphological changes in other organs or tissues of the Tam group compared with the no Tam group (Figures S6A and S6B). To further prove the key role of *Apj*<sup>+</sup> vessels in tumor growth, we used *Apj*-

*CreER;R26-GFP/DTA* and injected Tam 7 days after tumor cell transplantation. We found that ablation of *Apj*<sup>+</sup> vessels in established tumors could also inhibit tumor growth and angiogenesis (Figures S6C–S6E).

### The *Apj* Antagonist F13A Inhibits Tumor Angiogenesis and Growth

To further understand the pathological significance of *Apj* receptor activity in tumor blood vessels, and to evaluate its potential as a therapeutic target, we used the *Apj*-specific antagonist F13A to inhibit the Apelin-*Apj* system. F13A has been shown to reduce blood pressure in hypertension (Lee et al., 2005), promote liver regeneration (Yoshiya et al., 2015), and alleviate lung inflammation and injury during acute respiratory distress syndrome (Fan et al., 2015). Whether F13A could be used for inhibition of tumor growth has not been determined. Molecular dynamics simulation and structural analysis of the F13A-*Apj* complex model showed that F13A residue alanine (a substitution of the C-terminal phenylalanine) forms hydrogen-bond interactions with K268 and Y264 on helix VI of *Apj* (Figures 7A and 7B) via the peptide's terminal carboxyl group. In addition to this key hydrogen-bonding interaction, F13A engages other hydrophobic and polar



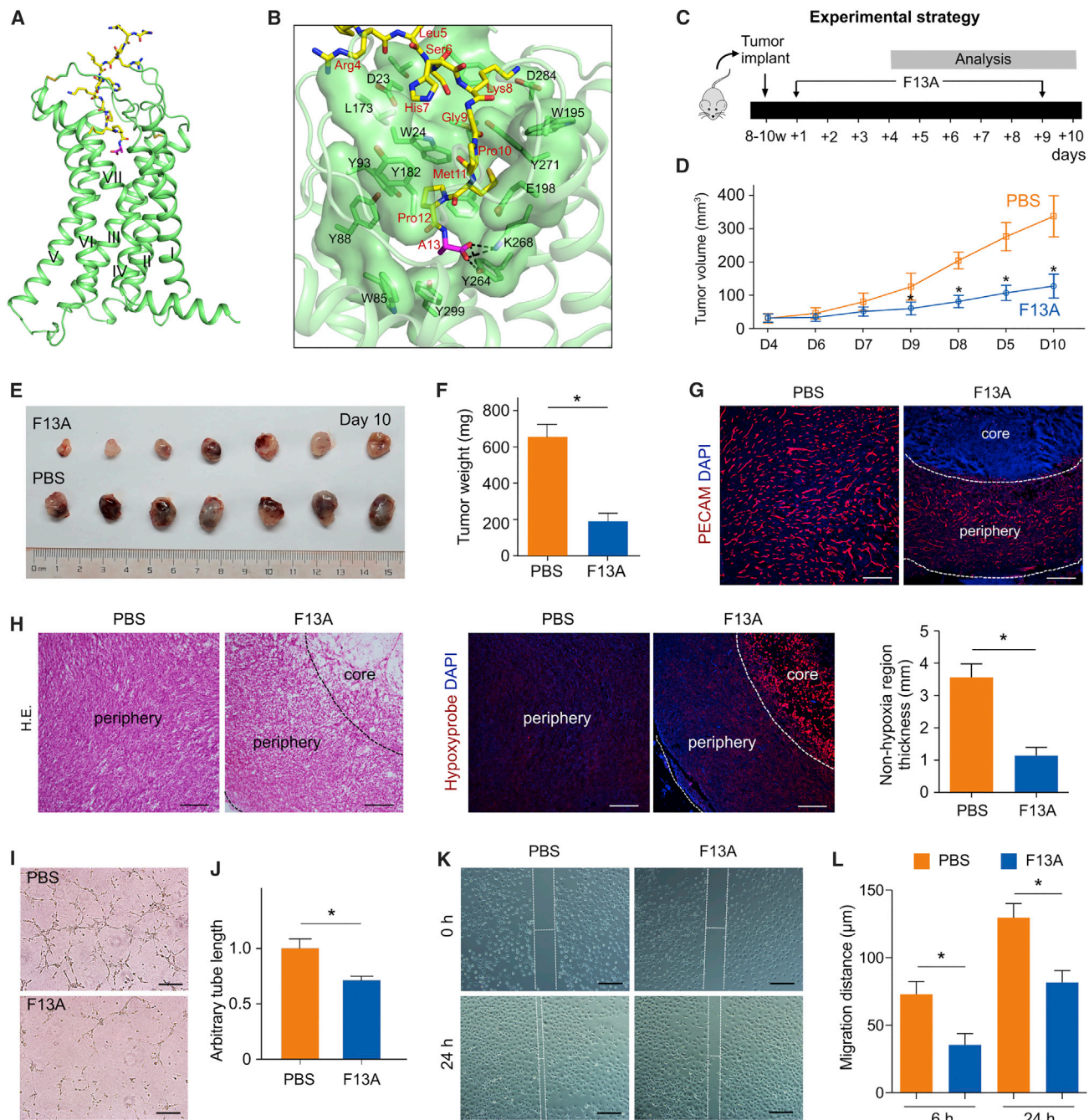


**Figure 7. Treatment of Apj Antagonist F13A Inhibits Tumor Angiogenesis and Growth**

(A) Structural model of F13A-Apj complex. Green cartoon for the receptor Apj and yellow sticks for the peptide ligand F13A. This model is derived from the molecular dynamics model of Apelin-13 (AP13)-Apj complex on the basis of the crystal structure of Apj-AMG3054 (PDB: 5VBL).

(B) Ligand-receptor binding interactions. F13A and Apj are labeled with red and black text, respectively. Magenta indicates F13A residue alanine (A13) that interacts with K268 and Y264 on Apj. Hydrogen-bonding interactions are indicated by black dashed lines.

(C) Schematic figure showing experimental strategy.

(D) Quantification of tumor volume (length  $\times$  width<sup>2</sup>/2 [mm<sup>3</sup>]) at indicated time after implantation. Student's t test was used to analyze differences, and values are shown as mean  $\pm$  SEM; \*p < 0.05; n = 8 for each time point.

(E) Pictures of tumors from PBS- or F13A-treated mice.

(F) Quantification of tumor weight in (E). \*p < 0.05. Data are mean  $\pm$  SEM; n = 8.

(G) Immunostaining for PECAM on tumor sections shows reduced vessel density in F13A-treated mice compared with PBS control.

(legend continued on next page)

interactions between the peptide ligand and Apj receptor. For example, the C terminus of the peptide ligand sits in a hydrophobic pocket composed of a cluster of aromatic residues: W24, W85, Y88, Y93, W195, Y264, Y271, and Y299. This pocket further contributes to the enhanced interaction network between F13A and the Apj receptor. On the basis of this structural analysis, we treated mice with F13A after tumor implantation and analyzed tumor samples 10 days later (Figure 7C). Tumor growth was significantly retarded in F13A-treated mice compared with PBS-treated mice (Figure 7D). Tissue samples collected at day 10 showed significant reductions in tumor volume ( $105.50 \pm 38.14$  versus  $332.30 \pm 62.17$  mm<sup>3</sup>, respectively) and weight ( $198.20 \pm 50.12$  versus  $632.04 \pm 92.39$  mg, respectively) in F13A-treated mice compared with controls (Figures 7E and 7F). Notably, there were large avascular regions in F13A-treated tumors compared with controls (Figure 7G). The core region of F13A-treated tumors was highly hypoxic, and the vascularized non-hypoxic region was significantly reduced in F13A-treated tumors compared with the PBS-treated controls (thickness  $3.51 \pm 0.48$  versus  $1.10 \pm 1.92$  mm, respectively; Figure 7H).

Previous studies showed that Apelin could stimulate the proliferation and migration of Müller cells, cultured ECs, and the retinal EC line RF/6A cells (Kasai et al., 2004; Lu et al., 2013). Using a Matrigel-based tube formation assay, we found that F13A-treated HUVECs showed a significant reduction in tube-like structures compared with PBS-treated HUVECs ( $0.66 \pm 0.05$  versus  $1.00 \pm 0.11$ , respectively; Figures 7I and 7J). Furthermore, scratch wound assays confirmed impaired migration of HUVECs by F13A treatment (6 hr,  $33.40 \pm 12.17$  versus  $57.71 \pm 13.05$   $\mu$ m, respectively; 24 hr,  $76.06 \pm 9.47$  versus  $132.20 \pm 15.23$   $\mu$ m, respectively; Figures 7K and 7L). A previous study demonstrated an important role for Apj in cardiac hypertrophy (Scimia et al., 2012). We systematically analyzed F13A- and PBS-treated heart samples. Echocardiography showed no significant difference in ejection fraction or fractional shortening between F13A- and PBS-treated groups (Figure S7A). Immunostaining for WGA and troponin I3 (TNNI3) on heart sections showed no significant difference in cardiomyocyte size between F13A- and PBS-treated groups (Figure S7B). In addition, we did not detect any observable change in vessel density or morphology in other organs examined histologically after F13A treatment (Figures S7C and S7D). Taken together, these *in vivo* and *in vitro* data demonstrate that F13A reduces tumor angiogenesis and inhibits tumor growth, without any adverse side effects on vascular homeostasis in other organs.

## DISCUSSION

In this study, we generated *Apj-DTRGFP-Luc* and *Apj-CreER* to investigate and to genetically target the tumor vasculature. We

found that Apj is minimally expressed in blood vessels of normal tissues but is significantly upregulated in tumor vessels. This is due to the hypoxic microenvironment in tumors that induces Apj expression, under the tight regulation of the VEGFA-VEGFR2 signaling pathway. VEGF is one of the HIF-1 target genes, and the VEGF-VEGFR2 signaling pathway has a key role in vascular development. In this study, we used our genetic tool to ablate VEGF/VEGFR2 signaling selectively in Apj<sup>+</sup> cells *in vivo* and found that it significantly inhibited angiogenesis and suppressed tumor growth. By two different genetic cell ablation strategies, we determined that these Apj<sup>+</sup> blood vessels are essential for tumor growth. Finally, treatment of tumor-bearing wild-type mice with the Apj antagonist F13A significantly impairs tumor angiogenesis and expansion. The *Apj-CreER* tool would be valuable to study gene function in pathological angiogenesis, as well as in development and tissue regeneration. Moreover, the newly generated *Apj-DTRGFP-Luc* offers a useful tool for intravital monitoring of actively sprouting vessels and pathological angiogenesis, such as in tumors. Its knockin DTRGFP cassette may also be useful to non-invasively assess the function of newly formed Apj<sup>+</sup> blood vessels in the settings of tumor, tissue injury, and regeneration.

Like its ligand Apelin, Apj is highly expressed in ECs of embryonic tissues. Previous studies showed that Apj<sup>+</sup> ECs form a primitive coronary plexus on the surface of the developing heart (Chen et al., 2014). Consistent with this, our *Apj-CreER* knockin mouse line confirmed that Apj is expressed in coronary ECs, but not in endocardial ECs, in the developing heart. However, very few Apj<sup>+</sup> vessels are detected in adult heart. We reason that the hypoxic environment of the uterus (Kimura et al., 2015), compounded by a rapid growth of embryonic tissues that outpaces formation of the vasculature, induces Apj expression in ECs of embryos. After birth, the heart and other organs are supplied with sufficient oxygen under normal conditions (Yutzev, 2014), thus reducing endothelial Apj expression. We also verified that the response of Apj<sup>+</sup> vessels to hypoxia is regulated by canonical VEGF signaling, which is also tightly regulated by tissue hypoxia (Liu et al., 1995), confirming that the hypoxic microenvironment of the tumor determines the activation of Apj and sprouting of Apj<sup>+</sup> vessels. We also confirmed that, under ischemic conditions such as hindlimb ligation and MI, ECs would respond to tissue hypoxia by upregulating Apj, and Apj<sup>+</sup> vessels were responsible for the injury-induced neovascularization in the infarcted tissues. Future studies are required to elucidate the cellular and molecular mechanism of Apj<sup>+</sup> vessel-mediated neovascularization in other pathological conditions and tissue regeneration.

Apj has pleiotropic roles in tumors, beyond those described in ECs. Apj has recently been found to influence the anti-tumor response of T cells via modulating JAK-STAT signaling in target cells (Patel et al., 2017). Apj was shown to interact with JAK1 to

(H) H&E staining, immunostaining for Hypoxyprobe on tumor sections shows thinner periphery and larger hypoxia core region and quantification of non-hypoxia region thickness. Data are shown as mean  $\pm$  SEM; \* $p < 0.05$ ;  $n = 8$ .

(I) Tube formation analysis by HUVECs cultured on Matrigel.

(J) Quantification of tube length per field. PBS-treated sample is set as 1. Data are shown as mean  $\pm$  SEM; \* $p < 0.05$ ;  $n = 4$ .

(K) Migration assay by scratch on cultured HUVECs.

(L) Quantification of migration distances at 6 and 24 hr after PBS or F13A treatment. Data are shown as means  $\pm$  SEM; \* $p < 0.05$ ;  $n = 4$ .

Scale bars, 200  $\mu$ m.

regulate interferon- $\gamma$  responses in tumors, and its functional loss reduces the efficacy of checkpoint-blocking immunotherapy (Patel et al., 2017). As a T cell effector cytokine, interferon- $\gamma$  could also modulate EC functions to induce tissue hypoxia and exhibit an anti-tumor effect (Kidoya et al., 2012). As Apj interacts with JAK1 to augment the interferon- $\gamma$  response, the anti-tumor effect could also be due to the increased response of tumor blood vessels to interferon- $\gamma$  and may thus improve the anti-tumor efficacy of T cells (Patel et al., 2017). Nevertheless, in our study we do not use the function of Apj for anti-tumor treatment; rather, we take advantage of its unique cell surface marker to distinguish tumor ECs for therapeutic targeting. This tumor-specific identifier could similarly be used for chimeric antigen receptor T cell-mediated immunotherapy, to direct engineered T cells with customized therapeutic reagents in future (Roybal et al., 2016).

Previous clinical data suggested that combined administration of chemotherapy and an anti-angiogenic treatment would yield maximal benefit (Teicher, 1996) because cytotoxic agents directly kill cancer cells, and anti-angiogenic agents kill cancer cells indirectly by depriving their supply of oxygen and nutrients. However, recent studies indicate that rather than promoting, anti-angiogenic therapy actually compromises the therapeutic benefit of anti-tumor drugs (Carmeliet and Jain, 2011). Because of the structurally and functionally abnormal nature of tumor vasculature, the interstitial hypertension of the tumor microenvironment, caused by tumor vessel leakiness and rapidly proliferating cancer cells, impairs the proper delivery of therapeutic drugs to solid tumors (Carmeliet, 2003). Restoring the imbalance between angiogenic stimulators and inhibitors would instead normalize the abnormal tumor blood vessels (Heath and Bicknell, 2009), and normalization of tumor blood vessels has been proposed as a new direction for treatment of solid tumors. It is proposed that although anti-angiogenic therapy initially normalizes tumor vessels, aggressive anti-angiogenic treatment results in a vasculature that is resistant to sufficient drug delivery (Jain, 2005). Although our study indicates that Apj<sup>+</sup> vessels could be directly targeted by F13A to reduce tumor growth, we found that F13A could not completely block tumor growth. Because tumor blood vessels are highly leaky and the interstitial pressure is high, it would be difficult to transfer drug effectively to all tumor regions. It would be important to combine F13A and cytotoxic chemotherapy to achieve improved therapeutic efficacy. Further studies on the time, dose, and delivery method of anti-angiogenic treatment are needed to optimize the efficacy of combined therapies.

In therapeutic drug development, small-molecule peptides are increasingly receiving attention because of their high specificity with relatively low toxicity. As such, F13A is an attractive drug, blocking the biological effects of Apelin, the key endogenous ligand for the Apj receptor. Previous work showed that F13A treatment could promote early-phase liver regeneration after partial hepatectomy, by activating Kupffer cells and increasing serum levels of TNF- $\alpha$  and IL-6 (Yoshiya et al., 2015). F13A therapy may facilitate efficient liver regeneration after liver surgery. In addition, F13A treatment augmented endogenous lung repair mechanisms after injury, as the Apelin-Apj axis is an intrinsic organ-protective mechanism to counteract the injury

response and to prevent lung damage (Fan et al., 2015). We demonstrate here that the repression of Apj activity by F13A could also block tumor angiogenesis and tumor development. A previous study using colorectal cancer cell lines showed that addition of F13A significantly reduced cancer cell proliferation (Picault et al., 2014), whereas our *in vivo* study indicates that the action of F13A could also be due to the inhibition of tumor angiogenesis, which leads to impaired tumor growth and expansion. Although the molecular mechanisms underlying this inhibition remain incompletely understood, our elucidation of the structural interaction between F13A and Apj may aid further investigation of the mechanisms of peptide binding and receptor blockade. Taken together, our study provides *in vivo* genetic evidence that the Apj receptor could serve as a functional marker of tumor angiogenesis and an important therapeutic target for drug development.

## STAR★METHODS

Detailed methods are provided in the online version of this paper and include the following:

- KEY RESOURCES TABLE
- CONTACT FOR REAGENT AND RESOURCE SHARING
- EXPERIMENTAL MODEL AND SUBJECT DETAILS
  - Model systems and permissions
  - Animals
  - Cell lines
- METHOD DETAILS
  - Methods: Mouse
  - Methods: Protein
  - Methods: Cell
- QUANTIFICATION AND STATISTICAL ANALYSIS

## SUPPLEMENTAL INFORMATION

Supplemental Information includes seven figures and can be found with this article online at <https://doi.org/10.1016/j.celrep.2018.10.015>.

## ACKNOWLEDGMENTS

We thank Shanghai Model Organisms Center (SMOC) and the Nanjing Biomedical Research Institute of Nanjing University for mouse generation; Dr. Richard A. Lang for providing DTRGFP cassette; and Baojin Wu, Guoyuan Chen, Zhonghui Weng, and Aimin Huang for animal husbandry. We also acknowledge technical help from Wei Bian, Tengfei Zhang, and members of the National Center for Protein Science Shanghai for assistance in microscopy. This work was supported by the Strategic Priority Research Program of the Chinese Academy of Sciences (CAS; XDB19000000 and XDA16020204), the National Science Foundation of China (31730112, 91639302, 31625019, 81761138040, 31571503, 31501172, 31601168, 31701292, 91749122, 81872241, 81872132, and 31801215), the National Key Research & Development Program of China (2018YFA0107900, 2018YFA0108100, 2016YFC1300600, 2017YFC1001303, and 2017YFA0505500), the Youth Innovation Promotion Association of CAS (2015218 and 2060299), the Key Project of Frontier Sciences of CAS (QYZDB-SSW-SMC003), the International Cooperation Fund of CAS, the National Program for Support of Top-Notch Young Professionals and Leading Talents, Shanghai Science and Technology Commission (17ZR1449600, 17ZR1449800, and 15XD1504000), the Shanghai Yangfan Project (16YF1413400 and 18YF1427600), the Rising-Star Program (15QA1404300), the China Postdoctoral Science Foundation (2016M600337, 2017M611634, 2017M621552, and 2016LH0042), the China Postdoctoral



Innovative Talent Support Program (BX201700267), China Young Talents Lift Engineering (YESS20160050 and 2017QNRC001), AstraZeneca, Boehringer Ingelheim, Sanofi-SIBS Fellowship, and Royal Society-Newton Advanced Fellowship (NA170109).

## AUTHOR CONTRIBUTIONS

H.Z. and B.Z. designed the study, performed experiments, and analyzed the data. X.T., L.H., Y.L., W.P., Q.L., J.T., J.W., and X.C. bred the mice, performed experiments, and provided valuable comments. Z.T. provided valuable comments and edited the manuscript. Y.L. and F.B. analyzed data from NIH online resources. Q.Z. and F.X. analyzed the crystal structure of F13A and Apj. N.S. provided valuable comments to this study and edited the manuscript. B.Z. supervised the study, analyzed the data, and wrote the manuscript.

## DECLARATION OF INTERESTS

The authors declare no competing interests.

Received: May 4, 2018

Revised: August 20, 2018

Accepted: October 3, 2018

Published: October 30, 2018

## REFERENCES

Ashley, E.A., Powers, J., Chen, M., Kundu, R., Finsterbach, T., Caffarelli, A., Deng, A., Eichhorn, J., Mahajan, R., Agrawal, R., et al. (2005). The endogenous peptide apelin potently improves cardiac contractility and reduces cardiac loading in vivo. *Cardiovasc. Res.* 65, 73–82.

Augustin, H.G., and Koh, G.Y. (2017). Organotypic vasculature: from descriptive heterogeneity to functional pathophysiology. *Science* 357, eaal2379.

Barnes, G., Japp, A.G., and Newby, D.E. (2010). Translational promise of the apelin–APJ system. *Heart* 96, 1011–1016.

Breitman, M.L., Clapoff, S., Rossant, J., Tsui, L.C., Glode, L.M., Maxwell, I.H., and Bernstein, A. (1987). Genetic ablation: targeted expression of a toxin gene causes microphthalmia in transgenic mice. *Science* 238, 1563–1565.

Carmeliet, P. (2003). Angiogenesis in health and disease. *Nat. Med.* 9, 653–660.

Carmeliet, P., and Jain, R.K. (2011). Principles and mechanisms of vessel normalization for cancer and other angiogenic diseases. *Nat. Rev. Drug Discov.* 10, 417–427.

Charo, D.N., Ho, M., Fajardo, G., Kawana, M., Kundu, R.K., Sheikh, A.Y., Finsterbach, T.P., Leeper, N.J., Ernst, K.V., Chen, M.M., et al. (2009). Endogenous regulation of cardiovascular function by apelin–APJ. *Am. J. Physiol. Heart Circ. Physiol.* 297, H1904–H1913.

Chen, H.L., Poduri, A., Numi, H., Kivela, R., Saharinen, P., McKay, A.S., Raftrey, B., Churko, J., Tian, X., Zhou, B., et al. (2014). VEGF-C and aortic cardiomyocytes guide coronary artery stem development. *J. Clin. Invest.* 124, 4899–4914.

Chng, S.C., Ho, L., Tian, J., and Reversade, B. (2013). ELABELA: a hormone essential for heart development signals via the apelin receptor. *Dev. Cell* 27, 672–680.

Cox, C.M., D'Agostino, S.L., Miller, M.K., Heimark, R.L., and Krieg, P.A. (2006). Apelin, the ligand for the endothelial G-protein-coupled receptor, APJ, is a potent angiogenic factor required for normal vascular development of the frog embryo. *Dev. Biol.* 296, 177–189.

D'Aniello, C., Lonardo, E., Iaconis, S., Guardiola, O., Liguoro, A.M., Liguori, G.L., Autiero, M., Carmeliet, P., and Minichiotti, G. (2009). G protein-coupled receptor APJ and its ligand apelin act downstream of Cripto to specify embryonic stem cells toward the cardiac lineage through extracellular signal-regulated kinase/p70S6 kinase signaling pathway. *Circ. Res.* 105, 231–238.

Dai, T., Ramirez-Correa, G., and Gao, W.D. (2006). Apelin increases contractility in failing cardiac muscle. *Eur. J. Pharmacol.* 553, 222–228.

Deshwar, A.R., Chng, S.C., Ho, L., Reversade, B., and Scott, I.C. (2016). The Apelin receptor enhances Nodal/TGF $\beta$  signaling to ensure proper cardiac development. *eLife* 5, 5.

Emsley, P., Lohkamp, B., Scott, W.G., and Cowtan, K. (2010). Features and development of Coot. *Acta Crystallogr. D Biol. Crystallogr.* 66, 486–501.

Eyries, M., Siegfried, G., Ciumas, M., Montagne, K., Agrapart, M., Lebrin, F., and Soubrier, F. (2008). Hypoxia-induced apelin expression regulates endothelial cell proliferation and regenerative angiogenesis. *Circ. Res.* 103, 432–440.

Fan, X.F., Xue, F., Zhang, Y.Q., Xing, X.P., Liu, H., Mao, S.Z., Kong, X.X., Gao, Y.Q., Liu, S.F., and Gong, Y.S. (2015). The Apelin–APJ axis is an endogenous counterinjury mechanism in experimental acute lung injury. *Chest* 147, 969–978.

Ferrara, N., and Kerbel, R.S. (2005). Angiogenesis as a therapeutic target. *Nature* 438, 967–974.

Forsythe, J.A., Jiang, B.H., Iyer, N.V., Agani, F., Leung, S.W., Koos, R.D., and Semenza, G.L. (1996). Activation of vascular endothelial growth factor gene transcription by hypoxia-inducible factor 1. *Mol. Cell. Biol.* 16, 4604–4613.

Guo, C., Yang, W., and Lobe, C.G. (2002). A Cre recombinase transgene with mosaic, widespread tamoxifen-inducible action. *Genesis* 32, 8–18.

Guy, C.T., Cardiff, R.D., and Muller, W.J. (1992). Induction of mammary tumors by expression of polyomavirus middle T oncogene: a transgenic mouse model for metastatic disease. *Mol. Cell. Biol.* 12, 954–961.

Haigh, J.J., Morelli, P.I., Gerhardt, H., Haigh, K., Tsien, J., Damert, A., Miquerol, L., Muhlner, U., Klein, R., Ferrara, N., et al. (2003). Cortical and retinal defects caused by dosage-dependent reductions in VEGF-A paracrine signaling. *Dev. Biol.* 262, 225–241.

Heath, V.L., and Bicknell, R. (2009). Anticancer strategies involving the vasculature. *Nat. Rev. Clin. Oncol.* 6, 395–404.

Ishida, J., Hashimoto, T., Hashimoto, Y., Nishiwaki, S., Iguchi, T., Harada, S., Sugaya, T., Matsuzaki, H., Yamamoto, R., Shiota, N., et al. (2004). Regulatory roles for APJ, a seven-transmembrane receptor related to angiotensin-type 1 receptor in blood pressure in vivo. *J. Biol. Chem.* 279, 26274–26279.

Ivanova, A., Signore, M., Caro, N., Greene, N.D., Copp, A.J., and Martinez-Barbera, J.P. (2005). In vivo genetic ablation by Cre-mediated expression of diphtheria toxin fragment A. *Genesis* 43, 129–135.

Jain, R.K. (2005). Normalization of tumor vasculature: an emerging concept in antiangiogenic therapy. *Science* 307, 58–62.

Jung, S., Unutmaz, D., Wong, P., Sano, G., De los Santos, K., Sparwasser, T., Wu, S., Vuthoori, S., Ko, K., Zavala, F., et al. (2002). In vivo depletion of CD11c<sup>+</sup> dendritic cells abrogates priming of CD8<sup>+</sup> T cells by exogenous cell-associated antigens. *Immunity* 17, 211–220.

Kálin, R.E., Kretz, M.P., Meyer, A.M., Kispert, A., Heppner, F.L., and Brändli, A.W. (2007). Paracrine and autocrine mechanisms of apelin signaling govern embryonic and tumor angiogenesis. *Dev. Biol.* 305, 599–614.

Kang, Y., Kim, J., Anderson, J.P., Wu, J., Gleim, S.R., Kundu, R.K., McLean, D.L., Kim, J.D., Park, H., Jin, S.W., et al. (2013). Apelin–APJ signaling is a critical regulator of endothelial MEF2 activation in cardiovascular development. *Circ. Res.* 113, 22–31.

Kasai, A., Shintani, N., Oda, M., Kakuda, M., Hashimoto, H., Matsuda, T., Hinuma, S., and Baba, A. (2004). Apelin is a novel angiogenic factor in retinal endothelial cells. *Biochem. Biophys. Res. Commun.* 325, 395–400.

Kidoya, H., Ueno, M., Yamada, Y., Mochizuki, N., Nakata, M., Yano, T., Fujii, R., and Takakura, N. (2008). Spatial and temporal role of the apelin/APJ system in the caliber size regulation of blood vessels during angiogenesis. *EMBO J.* 27, 522–534.

Kidoya, H., Kunii, N., Naito, H., Muramatsu, F., Okamoto, Y., Nakayama, T., and Takakura, N. (2012). The apelin/APJ system induces maturation of the tumor vasculature and improves the efficiency of immune therapy. *Oncogene* 31, 3254–3264.

Kidoya, H., Naito, H., Muramatsu, F., Yamakawa, D., Jia, W., Ikawa, M., Sonobe, T., Tsuchimochi, H., Shirai, M., Adams, R.H., et al. (2015). APJ regulates parallel alignment of arteries and veins in the skin. *Dev. Cell* 33, 247–259.

- Kimura, W., Xiao, F., Canseco, D.C., Muralidhar, S., Thet, S., Zhang, H.M., Abderrahman, Y., Chen, R., Garcia, J.A., Shelton, J.M., et al. (2015). Hypoxia fate mapping identifies cycling cardiomyocytes in the adult heart. *Nature* 523, 226–230.
- Klauda, J.B., Venable, R.M., Freitas, J.A., O'Connor, J.W., Tobias, D.J., Mondragon-Ramirez, C., Vorobyov, I., MacKerell, A.D., Jr., and Pastor, R.W. (2010). Update of the CHARMM all-atom additive force field for lipids: validation on six lipid types. *J. Phys. Chem. B* 114, 7830–7843.
- Kong, D., Li, Y., Wang, Z., Banerjee, S., and Sarkar, F.H. (2007). Inhibition of angiogenesis and invasion by 3,3'-diindolylmethane is mediated by the nuclear factor-kappaB downstream target genes MMP-9 and uPA that regulated bioavailability of vascular endothelial growth factor in prostate cancer. *Cancer Res.* 67, 3310–3319.
- Lampugnani, M.G. (1999). Cell migration into a wounded area in vitro. *Methods Mol. Biol.* 96, 177–182.
- Lee, D.K., Saldivia, V.R., Nguyen, T., Cheng, R., George, S.R., and O'Dowd, B.F. (2005). Modification of the terminal residue of apelin-13 antagonizes its hypotensive action. *Endocrinology* 146, 231–236.
- Liu, Y., Cox, S.R., Morita, T., and Kourembanas, S. (1995). Hypoxia regulates vascular endothelial growth factor gene expression in endothelial cells. Identification of a 5' enhancer. *Circ. Res.* 77, 638–643.
- Liu, Q., Hu, T., He, L., Huang, X., Tian, X., Zhang, H., He, L., Pu, W., Zhang, L., Sun, H., et al. (2015). Genetic targeting of sprouting angiogenesis using Aplin-CreER. *Nat. Commun.* 6, 6020.
- Lohela, M., Bry, M., Tammela, T., and Alitalo, K. (2009). VEGFs and receptors involved in angiogenesis versus lymphangiogenesis. *Curr. Opin. Cell Biol.* 21, 154–165.
- Lu, Q., Jiang, Y.R., Qian, J., and Tao, Y. (2013). Apelin-13 regulates proliferation, migration and survival of retinal Müller cells under hypoxia. *Diabetes Res. Clin. Pract.* 99, 158–167.
- Ma, Y., Yue, Y., Ma, Y., Zhang, Q., Zhou, Q., Song, Y., Shen, Y., Li, X., Ma, X., Li, C., et al. (2017). Structural basis for Apelin control of the human apelin receptor. *Structure* 25, 858–866.e4.
- Madisen, L., Zwingman, T.A., Sunken, S.M., Oh, S.W., Zariwala, H.A., Gu, H., Ng, L.L., Palmiter, R.D., Hawrylycz, M.J., Jones, A.R., et al. (2010). A robust and high-throughput Cre reporting and characterization system for the whole mouse brain. *Nat. Neurosci.* 13, 133–140.
- Palmiter, R.D., Behringer, R.R., Quaife, C.J., Maxwell, F., Maxwell, I.H., and Brinster, R.L. (1987). Cell lineage ablation in transgenic mice by cell-specific expression of a toxin gene. *Cell* 50, 435–443.
- Patel, S.J., Sanjana, N.E., Kishton, R.J., Eidizadeh, A., Vodnala, S.K., Cam, M., Gartner, J.J., Jia, L., Steinberg, S.M., Yamamoto, T.N., et al. (2017). Identification of essential genes for cancer immunotherapy. *Nature* 548, 537–542.
- Pauli, A., Norris, M.L., Valen, E., Chew, G.L., Gagnon, J.A., Zimmerman, S., Mitchell, A., Ma, J., Dubrulle, J., Reyon, D., et al. (2014). Toddler: an embryonic signal that promotes cell movement via Apelin receptors. *Science* 343, 1248636.
- Picault, F.X., Chaves-Almagro, C., Progetti, F., Prats, H., Masri, B., and Audigier, Y. (2014). Tumour co-expression of apelin and its receptor is the basis of an autocrine loop involved in the growth of colon adenocarcinomas. *Eur. J. Cancer* 50, 663–674.
- Pronk, S., Páll, S., Schulz, R., Larsson, P., Bjelkmar, P., Apostolov, R., Shirts, M.R., Smith, J.C., Kasson, P.M., van der Spoel, D., et al. (2013). GROMACS 4.5: a high-throughput and highly parallel open source molecular simulation toolkit. *Bioinformatics* 29, 845–854.
- Roybal, K.T., Williams, J.Z., Morsut, L., Rupp, L.J., Kolinko, I., Choe, J.H., Walker, W.J., McNally, K.A., and Lim, W.A. (2016). Engineering T cells with customized therapeutic response programs using synthetic Notch receptors. *Cell* 167, 419–432.e16.
- Ryan, H.E., Lo, J., and Johnson, R.S. (1998). HIF-1 alpha is required for solid tumor formation and embryonic vascularization. *EMBO J.* 17, 3005–3015.
- Sakimoto, S., Kidoya, H., Naito, H., Kamei, M., Sakaguchi, H., Goda, N., Fukamizu, A., Nishida, K., and Takakura, N. (2012). A role for endothelial cells in promoting the maturation of astrocytes through the apelin/APJ system in mice. *Development* 139, 1327–1335.
- Sastry, G.M., Adzhigirey, M., Day, T., Annabhimoju, R., and Sherman, W. (2013). Protein and ligand preparation: parameters, protocols, and influence on virtual screening enrichments. *J. Comput. Aided Mol. Des.* 27, 221–234.
- Sato, T., Suzuki, T., Watanabe, H., Kadowaki, A., Fukamizu, A., Liu, P.P., Kimura, A., Ito, H., Penninger, J.M., Imai, Y., and Kuba, K. (2013). Apelin is a positive regulator of ACE2 in failing hearts. *J. Clin. Invest.* 123, 5203–5211.
- Schulze, W., Hayata-Takano, A., Kamo, T., Nakazawa, T., Nagayasu, K., Kasai, A., Seiriki, K., Shintani, N., Ago, Y., Farfan, C., et al. (2015). Simultaneous neuron- and astrocyte-specific fluorescent marking. *Biochem. Biophys. Res. Commun.* 459, 81–86.
- Scimia, M.C., Hurtado, C., Ray, S., Metzler, S., Wei, K., Wang, J., Woods, C.E., Purcell, N.H., Catalucci, D., Akasaka, T., et al. (2012). APJ acts as a dual receptor in cardiac hypertrophy. *Nature* 488, 394–398.
- Seaman, S., Stevens, J., Yang, M.Y., Logsdon, D., Graff-Cherry, C., and St Croix, B. (2007). Genes that distinguish physiological and pathological angiogenesis. *Cancer Cell* 11, 539–554.
- Sheikh, A.Y., Chun, H.J., Glassford, A.J., Kundu, R.K., Kutschka, I., Ardigo, D., Hendry, S.L., Wagner, R.A., Chen, M.M., Ali, Z.A., et al. (2008). In vivo genetic profiling and cellular localization of apelin reveals a hypoxia-sensitive, endothelial-centered pathway activated in ischemic heart failure. *Am. J. Physiol. Heart Circ. Physiol.* 294, H88–H98.
- Teicher, B.A. (1996). A systems approach to cancer therapy. (Antioncogenics + standard cytotoxics → mechanism(s) of interaction). *Cancer Metastasis Rev.* 15, 247–272.
- Yoshiya, S., Shirabe, K., Imai, D., Tushima, T., Yamashita, Y., Ikegami, T., Okano, S., Yoshizumi, T., Kawanaka, H., and Maehara, Y. (2015). Blockade of the apelin-APJ system promotes mouse liver regeneration by activating Kupffer cells after partial hepatectomy. *J. Gastroenterol.* 50, 573–582.
- Yutzev, K.E. (2014). Cardiovascular biology: switched at birth. *Nature* 509, 572–573.

## STAR★METHODS

### KEY RESOURCES TABLE

REAGENT or RESOURCE	SOURCE	IDENTIFIER
<b>Antibodies</b>		
Goat anti-Mouse-GFP (FITC conjugate)	Abcam	Cat# ab6662
Rabbit anti-Mouse-Hypoxypore	Hypoxypore	Cat# HP3-100Kit
Rat anti-Mouse-PECAM	BD PharMingen	Cat# 553370
Rabbit anti-human-ESR	Abcam	Cat# ab32063
Mouse SMA (Tritc conjugate)	Sigma	Cat# C6198
Rabbit anti-Mouse-SM22a	Abcam	Cat# ab14106
Rabbit anti-Mouse-Calponin	Abcam	Cat# ab46794
Rabbit anti-Mouse-SMC-MHC	Abcam	Cat# ab53219
CLICK EDU ALEXA 555 IMAGING	Invitrogen	Cat# C10338
Goat anti-Mouse-Troponin I	Abcam	Cat# ab56357
WGA-Alexa 488	Invitrogen	Cat# W11261
Rabbit anti-Mouse-APJ	Pierce	Cat# PA521285
Mouse anti- $\beta$ -actin	Cell Signaling	Cat# 3700
Alexa donkey a-goat 555	invitrogen	Cat# A21432
Alexa donkey a-rabbit 555	invitrogen	Cat# A31572
Alexa goat a-rat 647	invitrogen	Cat# A21247
Alexa goat a-rat 555	invitrogen	Cat# A21434
HRP-anti-rabbit IgG	Jackson ImmunoResearch	Cat# 711-035-152
HRP-anti-mouse IgG	Jackson ImmunoResearch	Cat# 115-035-174
<b>Chemicals, Peptides, and Recombinant Proteins</b>		
F13A	Phoenix Pharmaceuticals	Cat# 057-29
Tam	Sigma	Cat# T5648
Matrigel	BD biocoat	Cat# 356237
DAPI	Sigma	Cat# D8417
Paraformaldehyde (PFA)	Sigma	Cat# 16005
Fluorescence-protecting mounting medium	Vector Lab	Cat# H-1800
Diethylnitrosamine (DEN)	Sigma	Cat# N0258
Dylight 594 Lycopersicon Esculentum lectin	Vector Lab	Cat# DL-1177
D-Luciferin	Cayman	Cat# 14681
Optimum cutting tissue (OCT)	Sakura	Cat# 4583
<b>Critical Commercial Assays</b>		
Hypoxia detection	Hypoxypore	Cat# Hypoxypore-1 Omni Kit
<b>Deposited Data</b>		
Raw data and analyzed data	This paper	N/A
<b>Experimental Models: Cell Lines</b>		
Mouse: lung tumor cells TC-1	The cell bank of Shanghai Institutes of Biological Sciences	N/A
Mouse: Hepatocarcinoma cells Hepa1-6	The cell bank of Shanghai Institutes of Biological Sciences	Cat# TCM39
Mouse: Lewis lung carcinoma cells LLC	The cell bank of Shanghai Institutes of Biological Sciences	Cat# TCM7
Human: Umbilical vein ECs HUVEC	ATCC	Cat# CRL-1730

(Continued on next page)



## Continued

REAGENT or RESOURCE	SOURCE	IDENTIFIER
Experimental Models: Organisms/Strains		
Mouse: APJ-CreER	Shanghai Model Organisms Center	N/A
Mouse: Apj-DTRGFP-Luc	Shanghai Model Organisms Center	N/A
Mouse: C57BL/6	The Jackson Laboratory	JAX: 000664
Mouse: R26-GFP	<a href="#">Madisen et al., 2010</a>	N/A
Mouse: MMTV-PyMT	Nicemice.org	J002374
Mouse: R26-DTA	<a href="#">Ivanova et al., 2005</a>	N/A
Mouse: VEGFR2-flox	<a href="#">Haigh et al., 2003</a>	N/A
Oligonucleotides		
primer1 of APJ-CreER: 5'-AGATACTCCCCCATCCCAAAG-3'	This paper	N/A
primer2 of APJ-CreER: 5'-CGCATAACCAGTGAAACAGCATTG-3'	This paper	N/A
primer3 of APJ-CreER: 5'-TCAGACTGGTTGTCAGCCCCATAG-3'	This paper	N/A
primer1 of Apj-DTRGFP-Luc: 5'-GCCAGAGGAAACCAGAGTGAACAG-3'	This paper	N/A
primer2 of Apj-DTRGFP-Luc: 5'-CCACAGCCAGGATAGTTGTATGG-3'	This paper	N/A
primer3 of Apj-DTRGFP-Luc: 5'-AGCAAGCACCCCTGAAGGATTGG-3'	This paper	N/A
Software and Algorithms		
ImageJ	NIH	<a href="https://imagej.nih.gov/ij/">https://imagej.nih.gov/ij/</a>
Prism 6	Graphpad	<a href="https://www.graphpad.com">https://www.graphpad.com</a>

## CONTACT FOR REAGENT AND RESOURCE SHARING

Further information and requests for resources and reagents should be directed to and will be fulfilled by the Lead Contact, Bin Zhou ([zhoubin@sibs.ac.cn](mailto:zhoubin@sibs.ac.cn)).

## EXPERIMENTAL MODEL AND SUBJECT DETAILS

### Model systems and permissions

All procedures were approved by the guidelines of Institutional Animal Care and Use Committee (IACUC) of the Institute for Nutritional Sciences, Institute of Biochemistry and Cell Biology, Shanghai Institutes for Biological Sciences, Chinese Academy of Sciences.

### Animals

All mice used were maintained on a C57BL6/J background (*MMTV-PyMT* were maintained on a C57BL6/J and FVB/n mixed background), both male and female between 8 and 10 weeks of age were randomly allocated to groups. No obvious sexual difference was detected within the parameters used for our experiments. *R26-GFP* ([Madisen et al., 2010](#)), *R26-DTA* ([Ivanova et al., 2005](#)), *VEGFR2-flox* ([Haigh et al., 2003](#)) mouse lines were described previously. *Apj-CreER* and *Apj-DTRGFP-Luc* mouse lines were generated using the CRISPR/Cas9 technology by Shanghai Model Organisms Center, Inc. (SMOC). Briefly, a cDNA encoding Cre recombinase fused with a mutant form of the estrogen receptor hormone-binding domain (CreER<sup>T2</sup>) ([Guo et al., 2002](#)) was targeted to the translational start codon ATG of *Apj* gene by homologous recombination. Similarly, cDNA encoding DTRGFP fusion protein ([Jung et al., 2002](#)) followed by luciferase was knocked into the endogenous ATG of *Apj* by homologous recombination. DNA encoding 2A cleavage peptide was inserted between DTRGFP and luciferase cDNA to allow simultaneous expression of the two cassettes. PCR primers spanning the genomic DNA were designed to test the correctly targeted allele. (*APJ-CreER*, 5'-AGATACTCCCCCATCCCAAAG-3', 5'-CGCATAACCAGTGAAACAGCATTG-3', 5'-TCAGACTGGTTGTCAGCCCCATAG-3'; *Apj-DTRGFP-Luc*, 5'-GCCAGAGGAAACCAGAGTGAACAG-3', 5'-CCACAGCCAGGATAGTTGTATGG-3', 5'-AGCAAGCACCCCTGAAGGATTGG-3'). Tam (Sigma, T5648) was dissolved in corn oil and introduced by gavage at the indicated time (0.1mg per gram of mice body weight). F13A (Phoenix Pharmaceuticals, 057-29) was dissolved in PBS (Invitrogen, 10010049) and was introduced by gavage at the indicated time (0.5 μg per gram of mice body weight per day). Control mice were injected with an equal volume of PBS. To assess EdU incorporation, mice were injected subcutaneously with EdU (Invitrogen, C10338, 10 μg per gram of mice body weight) dissolved in PBS 24 hours before sacrifice.

### Cell lines

All cell lines (Mouse lung tumor cells TC-1, Hepatocarcinoma cells Hepa1-6, Lewis lung carcinoma cells LLC and Human umbilical vein ECs HUVEC) were purchased from the cell bank of Shanghai Institutes of Biological Sciences and used for no more than

6 months after purchase. Cells were not re-authenticated but monitored for Mycoplasma contaminations. TC-1 was grown in RPMI-1640 (Invitrogen, 316421) plus 10% fetal bovine serum (Invitrogen, 10099141). Hepa1-6, LLC and HUVEC were all maintained in DMEM (Invitrogen, 11965092) with 10% fetal bovine serum. All cells were cultured in 5% carbon dioxide for at least 3 doublings before use. To study the influence of the hypoxic environment, HUVECs were moved to a hypoxic cell culture incubator that contained only 1% oxygen and analyzed 48 hours later.

## METHOD DETAILS

### Methods: Mouse

#### Xenograft tumor model

About  $5 \times 10^6$  tumor cells (TC-1, Hepa1-6 and LLC) were dissolved in 100  $\mu$ L RPMI-1640 or DMEM medium and mixed with 100  $\mu$ L Matrigel (BD, 356237) on ice. 8-10 weeks old adult male or female mice were anaesthetized using 10% chloralhydrate (3  $\mu$ g per gram of mice body weight, intraperitoneally) and maintained body temperature on a heated pad. Then the cell mix was immediately injected subcutaneously into the groin of each mouse by a 1ml injector. Tam (Sigma, T5648) or corn oil was administered 1 day later and tumor tissues were analyzed 10 days later. After whole-mount imaging, the tumor tissues were fixed in 4% paraformaldehyde (PFA, Sigma) for 1 hour, dehydrated in 30% sucrose (Sigma) overnight and then frozen for sectioning and immunostaining.

#### Orthotopic tumor model

About  $5 \times 10^6$  tumor cells (Hepa1-6) were collected and dissolved in 10-15  $\mu$ L DMEM medium and mixed with 20-30  $\mu$ L Matrigel (DMEM: Matrigel~1:2) on ice. For *in situ* liver injection, 8-10 weeks old adult male or female mice were anesthetized and then artificially ventilated with 2% isoflurane gas through tracheal intubation using an anesthetic gas machine (Harvard Apparatus) and a respiratory machine (Harvard Apparatus) on a constant heated 37°C pad. After their abdomen was shaved, a 1.5cm longitudinal incision was performed in the upper abdomen and the liver was exposed. Then immediately injected the cells into the left lobe of mice liver. After successful surgery, the abdominal skin was closed together layer by layer with a 5-0 suture. Similarly, the sham group were performed same surgery but without tumor cell injection. Tam or corn oil (No Tam) was given once at week 2 and once at week 3 after inoculation. Tumor tissues were analyzed 4 weeks later. After whole-mount imaging, the livers were fixed, dehydrated and frozen for sectioning and immunostaining.

#### DEN-induced hepatocarcinoma

Diethylnitrosamine (DEN, Sigma, N0258) was administered through intraperitoneal injection at 50  $\mu$ g per gram body weight to induce hepatocarcinoma (HCC) in 2-week-old newborn male or female mice. For lineage tracing of Apj<sup>+</sup> vessels, mice were orally gavaged with Tam once 24 weeks later and once 26 weeks later. Livers were collected for analysis at 28 weeks after DEN injection. After whole-mount imaging, the livers were fixed, dehydrated and frozen for sectioning and immunostaining.

#### MI

Briefly, 8-10 weeks old adult male or female mice were anaesthetized just as orthotopic tumor model procedure described above and their chests were shaved using a hair clipper. About 1cm longitudinal incision was made in the sternum and the heart was exposed using a retractor. Then the LAD coronary artery should occlude with a suture, at the upper 1/3 location of the artery. After successful or sham ligation, the chest cavity was closed with a 5-0 suture, and the thorax and skin also sutured together. The sham-operated group did the same operation but without LAD ligation. The surgery should do on a heating pad to maintain body temperature and kept warm for several hours after surgery. Tam (Sigma, T5648) or corn oil was administered 1 day later and heart tissues were analyzed 15 days later. After whole-mount imaging, the heart were fixed in 4% paraformaldehyde (PFA, Sigma) for 1 hour, dehydrated in 30% sucrose (Sigma) overnight and then frozen for sectioning and immunostaining.

#### Hindlimb ligation

Briefly, 8-10 weeks old adult male or female mice were anaesthetized using 10% chloralhydrate and placed in a supine position after they were nonresponsive, and then shaved their left hindlimbs with a hair clipper. An incision was made parallel to the femur and subcutaneous fat was removed. The underlying femoral artery was separated at the groin region and ligated by a 5-0 suture. Then the skin was sutured together. The sham-operated right hindlimb underwent the same operation but without ligation. The surgery should do on a heating pad to maintain body temperature. Tam (Sigma, T5648) or corn oil was administered 1 day later and hindlimbs were analyzed 10 days later. After whole-mount imaging, the hindlimbs were fixed in 4% paraformaldehyde (PFA, Sigma) for 1 hour, dehydrated in 30% sucrose (Sigma) overnight and then frozen for sectioning and immunostaining.

#### Hypoxia detection

For hypoxia detection *in vivo*, 8-10 weeks old male or female tumor cell injected mice were injected with Pimonidazole HCl (60~120  $\mu$ g per gram of body weight) 1 hour before killing according to the Hypoxyprobe-1 Omni Kit (Hypoxyprobe Inc.) protocol. Tumor tissues were collected in PBS and fixed in 4% PFA overnight at 4°C. After washing in PBS the next day, tissues were dehydrated in 30% sucrose, embedded in OCT and cryosectioned, followed by immunofluorescent staining, as previously mentioned above.

#### BS1-lection circulation detection assay

Briefly, adult tumor cell injected mice were anaesthetized with 10% chloralhydrate and placed in a supine position. After their abdominal fur was shaved, a 2-3cm longitudinal incision was performed in the abdominal region and the cavity was exposed. About 400  $\mu$ L

Dylight 594 Lycopersicon Esculentum lectin (Vector Lab, DL-1177) was then injected into the inferior caval vein 40 min with a 1ml injector before sacrifice, and then tumor samples were collected for analysis as described above.

### **Echocardiography**

Echocardiographic measurements were performed on adult mice via a digital ultrasound system (Vevo 2100 Imaging System, Visual Sonics) by a technician blinded to the experimental setup. Left ventricular fractional shortening (FS) and ejection fraction (EF) were obtained from the M-mode of short-axis view at the level of the papillary muscle. All parameters were obtained from at least 3 consecutive high-resolution cycles for analysis and all data were analyzed using original parameters and accompanying software.

### **Bioluminescence detection**

For *in vivo* luminescence of Firefly Luciferase, mice were anaesthetized with 10% chloralhydrate and injected with 150mg/kg of D-Luciferin (Cayman). Luciferase activity was measured using the Xenogen *in vivo* imaging system (IVIS; 1-minute medium binning), following the manufacturer's protocol.

### **Whole-mount microscopy**

For the whole-mount bright field and fluorescence imaging using the Zeiss stereo-microscope (AxioZoom V16), collected tissues were washed in phosphate-buffered saline (PBS, pH = 7.4) twice and set down gently on an agar gel in a Petri dish. Automated Z stack images were acquired to determine magnification of the boxed region.

### **Immunofluorescent staining**

In brief, tissues were collected in PBS, fixed in 4% paraformaldehyde (PFA, Sigma) for 0.5-1 hour at 4°C, then washed in PBS for 3 times at room temperature and dehydrated in 30% sucrose (Sigma) overnight at 4°C. Tissues were embedded in optimum cutting tissue (OCT, Sakura) for 1h at 4°C, then frozen in block with OCT and sectioned (Thermo HM525 cryosection machine) or stored at -80°C the next day. 10 µm-thick cryosections were collected on slides, washed in PBS for three times, incubated in 5% normal donkey serum (NDS) in PBST (PBS with 0.1% Triton X-100) for 0.5 hour at room temperature and incubated with primary antibodies diluted in 2.5% NDS diluted in PBST overnight at 4°C. All primary antibodies were commercially available reagents: GFP (Abcam, ab6662, 1:200), Hypoxyprobe (Hypoxyprobe Inc., HP3-100Kit), PECAM (BD PharMingen, 553370, 1:200), ESR (Abcam, ab32063, 1:1), SMA (Sigma, C6198), SM22a (Abcam, ab14106), Calponin (Abcam, ab46794), SMC-MHC (Abcam, ab53219), EdU (Invitrogen, C10338), Troponin I (Abcam, ab56357), WGA-Alexa 488 (Invitrogen, W11261, 1:100). After washing out primary antibodies, signals were then developed with Alexa fluorescent antibodies (Invitrogen) for 0.5 hour at room temperature and nuclei were stained with DAPI. After slides were rinsed with PBS, they were mounted with fluorescence-protecting mounting medium (Vector Lab). Images were obtained by a Zeiss confocal microscopy system (Zeiss LSM 710) and image data were analyzed by ImageJ (NIH) software.

### **H&E staining**

10-µm-thick cryosections were incubated in Hematoxylin A solution for 3 min, washed with running tap water for 1 min, rinsed in 1% concentrated hydrochloric acid diluted in 70% ethanol for 1 min and washed with water for 1 min. Then the slides were incubated in 1% ammonia water for 1 min, washed for 1 min, stained with Eosin-Y solution for 8 s, dehydrated in a series of ethanol and xylene, and lastly mounted with neural balsam. All Image data were acquired using an Olympus microscope (Olympus, DP72).

### **Western Blotting**

After culture in a hypoxic environment for 48 hours, HUVECs were homogenized in Tris-SDS lysis buffer (50 mM Tris-HCl pH8.0 and 1% SDS) with protease inhibitors (Roche, 11836153001), incubated for 30 min on ice, and then centrifuged at 22,000 g for 15 min to isolate the protein supernatant. All samples were mixed with 5x loading buffer (10% SDS, 0.3M Tris-HCl pH6.8 and 1.5M dithiothreitol), boiled for 7-8 min, resolved via SDS-PAGE on 10% gels (Life Technologies, NP0322BOX) and transferred onto polyvinylidene difluoride membranes (Millipore, IPFL00010) through a Mini Trans Blot system (Bio-Rad). Then the membranes were blocked with PBS-T (10mM Tris-HCl pH8.0, 150mM NaCl and 0.5% Tween-20) and 5% skimmed milk powder for 1 hour at room temperature. After that, membranes were incubated with indicated primary antibodies overnight at 4°C, washed for 3 times, and incubated with HRP-conjugated secondary antibodies for 1 hour at room temperature. Protein signals were detected via enhanced chemiluminescence kit (Pierce), according to manufacturer's protocol. All antibodies were commercially available: anti-APJ (Pierce, PA521285, 1:500), anti-β-actin (Cell Signaling, 4970L, 1:1000), HRP-anti-rabbit IgG (Jackson ImmunoResearch, 711-035-152, 1:4000), HRP-anti-mouse IgG (Jackson ImmunoResearch, 115-035-174, 1:4000).

## **Methods: Protein**

### **Molecular dynamics simulations of F13A-APJ complex**

The simulated AP13-APJ complexes were embedded in a hydrated lipid POPC bilayer and solvated by TIP3P waters with 0.15M NaCl. The CHARMM36-CAMP force field (Klauda et al., 2010) was adopted for protein, lipid, water molecules and ions. Molecular dynamics simulations were performed using Gromacs 5.1.2 (Pronk et al., 2013), as previously described (Ma et al., 2017). Based on the crystal structure of APJ-AMG3054 (PDB: 5VBL) (Ma et al., 2017), the initial conformation of AP13 with APJ was obtained by gradually mutating AMG3054 to AP13 by multiple rounds of single residue modification/mutation and energy minimization using the Protein Preparation Wizard (Sastry et al., 2013). AP13 was finally mutated to F13A in the F13A-APJ complex structural model using COOT (Emsley et al., 2010) and further energy minimized using BioLuminate and Prime in the Schrödinger suite. The figures were generated using PyMol.



## Methods: Cell

### HUVECs migration assay

Migration assay was performed and developed according to the previously published protocol (Lampugnani, 1999). Briefly, HUVECs were seeded onto 24-well cell culture plates at a density such that they could reach ~80% confluence after 24 hours' incubation. The HUVEC monolayer was slowly and gently scratched with a new 1 ml pipette tip across the center and in one direction. The tip's long axis should always be perpendicular to the surface of the well to ensure equal gap distance. After that, the wells were washed twice gently and replenished with fresh medium. The F13A groups were supplemented with F13A (500ng/ml, resolved in PBS previously) and control groups were supplemented with an equivalent volume of PBS. After 6 hour and 24 hour incubation, the cells were visualized via a light microscope (Olympus), multiple views of each well were taken using the Scion Image software, and all gap distances were quantitatively evaluated using ImageJ software.

### HUVECs tube formation assay

Tube formation assay *in vitro* was performed based on modifications according to the previous publication (Kong et al., 2007). The HUVECs were starved for 6 hour before tube formation assay in serum-free DMEM medium without antibiotics. The 24-well plate was coated with Matrigel (be careful of bubble formation) and polymerized for at least 1 hour on a level surface at room temperature. After that, HUVECs were trypsinized, concentrated, resuspended by pipetting up and down to ensure a homogeneous single-cell suspension, and then seeded to the 24-well plate at an appropriate concentration. The F13A groups were supplemented with F13A (500ng/ml, resolved in PBS previously) and control groups were supplemented with an equivalent volume of PBS. After 12 hours' incubation, the cells were visualized via a light microscope (Olympus), and images of the capillary network were taken using the Scion Image software.

## QUANTIFICATION AND STATISTICAL ANALYSIS

All mice were randomly assigned to different groups and all data were obtained from 4-8 individual samples, as indicated in each experiment. For all experimental data, all calculation analysis were performed by Prism (GraphPad software, La Jolla, CA). In both animal and cell experiments, unpaired two tailed Student's t tests were performed to analyze the P value for single comparison between two groups (Figure 2I,M; Figure 3E; Figure 4C,H; Figure 5F,H,J; Figure 6C,H; Figure 7D,F,H,J,L; Figure S6D), and two-way ANOVA were used for multiple comparisons (Figure 4E,F; Figure 6E,F; Figure S3E,I). N represents number of animals in animal experiments and number of replications in cell experiments. Significance was accepted when  $p < 0.05$ . All data are presented as mean  $\pm$  SEM. All of the statistical details of experiment can be found in the figure legends and results part.